

Fermi National Accelerator Laboratory

TM-1541

Design Study of a Medical Proton Linac for Neutron Therapy*

Shinji Machida and Deepak Raparia
Texas Accelerator Center/University of Houston
2319 Timberloch Place
The Woodlands, Texas 77380

August 26, 1988

*To appear in part in papers to be presented at the 1988 Linear Accelerator Conference, Williamsburg, Virginia, October 3-7, 1988 and at the Tenth Conference on the Application of Accelerators in Research and Industry, University of North Texas, Denton, Texas, November 7-9, 1988



Operated by Universities Research Association Inc. under contract with the United States Department of Energy

Design Study of a Medical Proton Linac for Neutron Therapy

Shinji Machida and Deepak Raparia

Texas Accelerator Center/University of Houston
2319 Timberloch Place
The Woodlands, Texas 77380

August 26, 1988

Contents

1	Introduction	1
2	Systems	2
2.1	Low Energy Beam Transport (LEBT)	2
2.2	Radio Frequency Quadrupole (RFQ)	3
2.2.1	Choice of Parameters	4
2.2.2	Beam Dynamics Calculations	5
2.2.3	RFQ Structure and Power	6
2.2.4	Matching the RFQ to the DTL	7
2.3	Drift Tube Linac (DTL)	8
2.3.1	Cavity Specifications	8
2.3.2	RF Properties	10
2.3.3	RF Power Considerations	13
2.3.4	Beam Dynamics Calculations	14
3	Conclusion	19
	Acknowledgements	20
	References	21
	Appendices	23
A	Some Clinical Options	23
A.1	Motivation	23
A.2	2.3 MeV Beam Transport through the DTL	24
A.3	Isotope Production	24
B	RFQ Options	25
B.1	RFQ Structures	25
B.1.1	Four Vane	25
B.1.2	Four Rod	25
B.1.3	TAC Design	26
B.2	Matching to the DTL	26
B.2.1	Option 1	26
B.2.2	Option 2	27

C SUPERFISH Design Code	27
D Beam Dynamics Codes	28
D.1 Example of GENLIN Output	29
D.2 Comparison of the Basic Lattice	29
D.3 Treatment of Space Charge	29
D.4 Longitudinal-Transverse Coupling	30
D.5 Permanent Magnet Quadrupoles	30
Figure Captions	33

1 Introduction

In early 1988 administrators and physicians at Rush Presbyterian St.-Luke's Medical Center decided to pursue the possibility of building a neutron therapy facility at Rush. Their decision was greatly influenced by the encouraging clinical results reported at Fermilab's Neutron Therapy Facility. They were also aware of the excellent reliability of the Fermilab linac, which supplies the protons for the facility's beryllium production target. However, because of the linac's size and unavailability from a commercial source, they believed their only option for obtaining a proton generator was to purchase a commercially available medical cyclotron. In response to this issue some Fermilab staff members described a scenario [1] in which a proton linac for medical purposes compared favorably with commercially available cyclotrons. This linac would provide 66 MeV protons with a peak current of 50 milliamps at a 60 Hertz rate and a 60 microsecond pulse width. The linac tank would be about 40 cm in diameter and the machine length, including source, low energy beam transport (LEBT), and radiofrequency quadrupole (RFQ), would be about 70 feet. Power consumption was estimated to be 200 kW.

This paper describes a design study which establishes the physical parameters of the LEBT, RFQ, and linac, using computer programs available at Fermilab. Beam dynamics studies verify that the desired beam parameters can be achieved. The machine described here meets the aforementioned requirements and can be built using existing technology. Appendix A explores other technically feasible options which could be attractive to clinicians, though they would complicate the design of the machine and increase construction costs. One of these options would allow the machine to deliver 2.3 MeV protons to produce epithermal neutrons for treating brain tumors. A second option would provide 15 MeV protons for isotope production.

2 Systems

2.1 Low Energy Beam Transport (LEBT)

One of the most commonly used and reliable proton sources is the duoplasmatron [2]. The technology of this source is well developed, and duoplasmatrons can be easily constructed or obtained commercially. The proton kinetic energy from the duoplasmatron is assumed to be 30 keV in the following.

The beam from an ion source is relatively large in radius and divergence and must be matched to the radio frequency quadrupole (RFQ). Lenses are required to focus the beam onto the RFQ entrance. There are two common choices of lens for beam energies below 100 keV, namely the solenoid and the electrostatic lens. In the case of the Loma Linda medical accelerator [3][4], solenoid lenses are being considered. With solenoid lenses the length of the low energy beam transport (LEBT) line will be approximately one meter, which is rather long. In the case of solenoid lenses the beam may be neutralized by background gas which reduces the space charge effect. The neutralization time constant depends upon pressure. During this neutralization time the space charge forces change. Because of this the beam phase space ellipse rotates, making it difficult to match the beam to the RFQ acceptance. On the other hand, there is no space charge neutralization in the case of electrostatic lenses and the length of the LEBT is greatly reduced (22 cm). Einzel lenses are simple to fabricate, require minimal space and require no power and no cooling in comparison with magnetic focusing (solenoids) and no extra power supply. The excitation of these lenses can be derived from a high-voltage divider system on the ion-source power supply.

The LEBT consists of two Einzel lenses. Two lenses were chosen to provide two degrees of freedom to match to the RFQ acceptance. (Two degrees of freedom are sufficient for the matching requirement). The present design provides 5 cm of space between the lenses for a steering magnet and beam diagnostic elements. The calculations for these lenses are shown in Fig 1. Calculations were done using the program AXCEL [5], which includes space charge and ion image calculations. In these calculations there was no space charge neutralization. Since it is very difficult to know the actual

boundary values, it is necessary to provide the freedom for longitudinal movement of the lenses. This can be done by using three bellows in between the lenses. It is worth noting that the ratios of beam radius to lens bore are 1:2 and 1:3 in the first and second lenses, respectively. The gap between the high voltage electrode and ground electrode is one cm, which is large enough to hold the high voltage (30 kV). The main parameters of the LEBT are shown in Table 1.

Table 1: Lens Parameters

1st Lens	
Voltage	29.45 kV
Length	7.2 cm
Spacing between electrodes	1.0 cm
2nd Lens	
Voltage	29.3 kV
Length	6.2 cm
Spacing between electrodes	1.0 cm

Because of spherical aberrations in electrostatic lenses, approximately 90% of the beam can be focused into the RFQ acceptance. For proper beam matching it is required to have better than .1% voltage regulation, which can be done with present technology. With this lens system H_2^+ and H_3^+ cannot be separated. They may represent 30% of the beam but should cause very little extra space charge effect in the RFQ, which has a space charge current limit of 100 mA.

2.2 Radio Frequency Quadrupole (RFQ)

A radio frequency quadrupole (RFQ) is selected to accelerate protons up to 2.3 MeV because it is a simple device and does the job of acceleration, bunching and focusing simultaneously, with minimum injection energy and minimum emittance growth. It produces

a strong electric quadrupole field near the axis. The transverse components of this field (uniform in space and alternating in time) give rise to a strong, alternating-gradient focusing effect that can focus ion beams traveling along the axis of the structure. By scalloping the vane-tip geometry, a longitudinal component is introduced into the electric field near the axis that can be used to bunch and accelerate the ions.

The RFQ contains four regions: the radial matching section, the shaper, the gentle buncher, and the acceleration section. In the radial-matching region, the vane aperture is tapered to adjust the focusing strength from almost zero to its full value in a few cells. This allows the DC injected beam to be matched into the time-dependent focusing of the RFQ. In the shaper the acceleration efficiency, A , and the synchronous phase increase linearly to bunch the beam. In the gentle buncher, the modulation is increased such that the longitudinal small oscillation frequency at zero current and the spatial length of the separatrix remain constant, and the beam is adiabatically bunched as it accelerates. In the acceleration section, modulation and phase angle are conventionally kept constant [6]. In the present design the modulation is increased in order to keep the transverse current limit more than 100 mA. This results in the same transmission efficiency and same emittances but a 33 % shorter length than a conventional RFQ. The higher longitudinal field gradient (3.97 MV/m) makes matching the RFQ to the drift tube linac (DTL) easier.

2.2.1 Choice of Parameters

The frequency for this RFQ is chosen to be 425 MHz for reasons of RF power source availability and the beam current (50 mA) requirement [7]. The bravery factor is 2.2 Kilpatrick for this design [8]. Sparking rates can only be crudely estimated, and at this voltage (112.5 kV) the sparking rate is approximately 0.2 spark per day [9]. The injection energy is 30 keV (energy from ion source) and is sufficient for this current [7]. The output energy is 2.3 MeV which is selected for producing epithermal neutrons (see Appendix A). The bore radius is 3mm to accommodate the beam emittance from the LEBT as well as to provide adequate alignment tolerances and opti-

mization of the RFQ length which, in the present design, depends on the transverse space charge current limit. The bore radius of 3 mm is also required for the 40 degree transverse phase advance (zero current), which is approximately the same phase advance per unit length as in the drift tube linac (DTL). This condition is required for easier transverse matching between the RFQ and the DTL. The main parameters are shown in Table 2.

Table 2: RFQ Parameters

Frequency	425 MHz
Ion	Proton
Number of cells	131
Length	100.67 cm
Vane voltage	112.5 kV
Bravery Factor	2.2 Kilpatrick
Average Radius	3 mm
Final Modulation	3.7
Final synchronous phase	-30 deg
Transverse phase advance	40 deg
Longitudinal phase advance	18 deg

2.2.2 Beam Dynamics Calculations

The RFQ performance was analyzed with the RFQ-linac design and simulation code RFQSCOPE [10] and PARMTEQ [6]. The acceptance is 0.75π mm mrad. Transmission for zero current is 98% and for 50 mA it is 92%. Table 2 shows the main parameters for the RFQ and Fig. 2 shows the beam size, phase and energy profiles. Fig. 3 shows the input and output beam emittances in all three planes. The emittance growth for 90% of the beam is 32% as shown in the simulation results of Table 3.

Table 3: Simulation Results

Transmission	
50 mA	92 percent
0 mA	96 percent
Emittance	
(90 percent [rms])	
(pi cm mm)	
x-xp	.0464 [.0101]
y-yp	.0439 [.0104]
phi-w	.8166 [.1746]
Emittance growth	
(90 percent)	32 percent

2.2.3 RFQ Structure and Power

We have three choices for the RFQ structure: (1) Four vane [6]: this structure is conventional and has some voltage stabilization problems (which can be removed by using different coupling rings), and it is complicated to fabricate in comparison with the following structures. (2) Four rod (University of Frankfurt design)[11]: this design does not have the voltage stabilization problems, and it is easier to fabricate. The power requirement is higher than for structures (1) and (3). (3) TAC design[12]: this structure was recently developed at the Texas Accelerator Center (Fig. 4). It is very simple to fabricate, is smaller in size, and has a lower power requirement. It has no voltage stabilization problems. Table 4 shows a comparison of these structures (for detailed calculations see Appendix B).

For each of these structures the power is less than 210 kW and the beam power is 115 kW. For this purpose we can use the same rf tube which is used in the case of the Loma Linda RFQ[13].

Table 4: RFQ Structures

Structure Characteristic	Four Vane	Four Rod	TAC design

Voltage stabilization problem	yes	no	no
Fabrication	complicated	simple	simple
Tank diameter(cm)	15	30	20
Power(kW)	190	210	200
Quality Factor	11000	8600	8800

2.2.4 Matching the RFQ to the DTL

The beam from the RFQ should be matched to the DTL acceptance for the design current (50 mA) in all three planes. There are three ways to match the beam to the DTL: (1) In this method the matching section consists of three quadrupoles and one rf gap (buncher). All three planes can be matched exactly. (2) This method requires four more RFQ cells at the end of the RFQ and a half length quadrupole in the DTL. The transverse planes can be matched exactly with fairly good matching in the longitudinal plane. (3) This method requires only four RFQ cells. We will call this section a post radial matching section, PRMS. The transverse planes can be matched for the both zero current and full current (50 mA) with fairly good matching in the longitudinal plane. We will discuss here only the last method. The other two will be discussed in Appendix B.

The vane in the PRMS is modified such that it tapers out (with no modulations), as shown in Fig. 5 and provides the transverse matching condition at zero current for the DTL acceptance. The DTL is about 10 cm away from last cell in the PRMS (Fig. 6). Fig. 7 shows the experimental and simulation results [14] for the Los Alamos RFQ. If we increase the voltage from the design voltage by 10 % , the transmission efficiency remains almost the same and the phase space ellipse rotates. We use this fact to match the ac-

ceptance of the DTL at full current (Fig. 8). This method produces a mismatch factor (as defined in TRACE3D) in the longitudinal plane of 1.4. The phase spread is 45 degrees, which is smaller than the rf bucket width (91 degrees, synchronous phase -30 degrees) of the DTL.

2.3 Drift Tube Linac (DTL)

2.3.1 Cavity Specifications

The most general figure of merit for an accelerating cavity is the shunt impedance. The shunt impedance is defined as

$$Z = \frac{E_0^2}{P_0/L},$$

where E_0 is the average accelerating field gradient, P_0 is the power loss and L is the cavity length. It represents how high a field we can produce with a certain power per unit length. In a proton linear accelerator, and in general in any cavity using a standing wave, we only use the electric field component having the same phase velocity as a particle. Taking this into account, a more convenient quantity is the effective shunt impedance,

$$Z_{TT} = \frac{(E_0 \cdot T)^2}{P_0/L},$$

where T is called the transit time factor

$$T = \frac{1}{E_0 \cdot L} \int dz E_0 \cos kz.$$

Here k is the wave number of the RF.

In the following procedure for the structure design, we try to find the dimensions of the cavity which result in the largest effective shunt impedance. But at the same time, we have to consider the ratio of the maximum field gradient E_s to the average field E_0 to avoid sparking. Also some technical issues should be considered so that the design would be a feasible one.

In order to estimate the various quantities of the RF cavity, namely the resonant frequency, shunt impedance, maximum field

gradient and so on, SUPERFISH is most commonly used. The SUPERFISH code assumes an axially symmetric cavity. Although in the case of the DTL structure, the supporting stem breaks the axial symmetry, we first calculate these quantities without the stem and later introduce the effect of it as a perturbation. Many experimental results show that this procedure is good enough because the electric field line is perpendicular to the stem at the place where the stem is installed. A description of the use of SUPERFISH for this design is given in Appendix C.

As the tank radius is inversely proportional to the resonant frequency, the choice of 425 MHz makes the diameter about a half that of a DTL operated at 200 MHz. Figure 9 shows the relation between the tank radius and the effective shunt impedance at certain $\beta(=v/c)$. At each β there is a maximum. In this design, because of the desire for simplicity of the RF power system and tank fabrication, the whole DTL should be constructed as one tank. As a result of the compromise among the different optimum points with β , we chose 21 cm as the tank radius.

Figure 10 shows that the smaller the drift tube (DT) radius, the higher the effective shunt impedance. But the electric field concentration on the DT also makes a higher maximum field gradient E , on the nose corner as shown in Fig. 11. Besides that, we have to allow enough room to install a quadrupole magnet inside the DT. The radius of a quadrupole would be the same independent of energy, so it might be better not to change the DT radius with β . We chose 4 cm as the DT radius, which seemed to be adequate.

Figure 12 shows that a smaller stem radius improves the effective shunt impedance. But there are some constraints on its size. First, the stem must have enough mechanical strength to support the DT. Secondly, in order to install a water pipe to cool the DT, it should have a large enough cross section. From these considerations, we chose 0.5 cm as the stem radius.

Figure 13 shows that the smaller the nose corner radius is, the higher the shunt impedance is taking β as a parameter. But from the point of view of the maximum field gradient, there is the minimum point in each β curve as shown in Fig. 14. Moreover, if the nose corner radius is reduced below a certain value, the maximum field point moves to the bore nose corner and increases rapidly. In the

case of the nose corner radius, we can change its value with β . We chose 0.5 cm from $\beta=0.065$ to 0.150, 1.0 cm from $\beta=0.150$ to 0.250 and 2.0 cm from $\beta=0.250$ to 0.350, respectively. The only problem with changing the radius with β is the frequency adjustment at the transition point. But this is not so serious because one might be able to estimate it by using the computer code for the field calculation.

The bore radius is the most important dimension in the DTL because it determines the acceptance. Therefore we cannot decide its value without an estimation of the beam dynamics. Here we chose 0.5 cm because of the proportional reduction of the tank radius compared with a 200 MHz DTL. It must be reexamined after the beam dynamics study.

Workers at Los Alamos proposed a tilted drift tube face to increase the effective shunt impedance. But we did not adopt this idea because it might add some mechanical and alignment complexity.

The bore corner radius is chosen 0.3 cm. There is no strict reason to choose this value.

Figure 15 shows the individual cell geometry and its electric field lines ($H_\phi = \text{const}$) at certain β . In the shortest cell, the mechanical tolerance is also indicated. The error value corresponds to a change of the resonant frequency of 0.1 MHz. From this we notice that the DT length must be precisely machined but the bore radius need not be. Figures 16 and 17 show the effective shunt impedance and the maximum field as a function of β , respectively. From these figures, we can see that ZTT has a maximum value at about $\beta=0.15$ (Energy=10 MeV) and decreases on the both sides. After $\beta=0.15$, the maximum field gradient decreases with increasing β . The step changes at $\beta=0.15$ and 0.25 in both figures are due to the transition of the nose corner radius.

2.3.2 RF Properties

Based on the optimized dimensions of each individual cell, we can design the whole linac system. If the required beam parameters are determined and the average field gradient E_0 is fixed by some constraint, we can estimate the RF parameters, especially peak and average RF power. Then the detailed dimensions of the whole structure are determined for the beam dynamics study and construction.

These procedures are done by using the computer code GENLIN in PARMILA (Appendix D).

The beam requirements of this DTL are shown in Table 5.

Table 5: Main Beam Parameters

Output Peak Current	50	mA
Repetition Rate	60	Hz
Beam Width	60	micro sec
Input Energy	2.3	MeV
Output Energy	66	MeV

To make a compact machine, it is obvious that we should take as high a field gradient as possible. But there are some factors that limit E_0 . Above a certain value of E_0 , the possibility of sparking increases rapidly. To estimate this phenomena there is an empirical law called the Kilpatrick limit [8]. Although there are many different interpretations of this law and it, in fact, should depend on the details of each individual case, usually we take between one and two times this value as the sparking limit. The Kilpatrick limit is a function of frequency, and is about 20 MV/m at 425 MHz. Table 6 shows the ratio of the maximum field gradient to this limit and the expected sparking rate per day using a formula of R.J.Noble [9] for a range of average field gradients.

Table 6: Ratio of the Maximum Field E_s to the Kilpatrick Field E_k and Probability of Sparking.

Average Field E_0	Ratio E_s/E_k	Probability
4 MV/m	1.3	0.7 sp/day
5	1.6	4.0
6	1.9	33.

From the point of view of the beam dynamics, E_0 determines the strength of the longitudinal restoring force. It determines the longitudinal acceptance but in combination with the transverse restoring force it can result in a coupling resonance condition. We will mention this more in the section on beam dynamics.

As the first iteration, we chose 5 MV/m for E_0 mainly because of the ratio to the Kilpatrick limit and the sparking estimates. The sparking probability was calculated to be about four sparks per day.

The GENLIN subroutine in PARMILA produces the whole DTL parameter table (Appendix D), when provided with the SUPERFISH output parameters like the shunt impedance and transit time factor and the beam and RF factors like E_0 . Table 7 shows the summary of the parameters of this DTL system. The peak and average RF power includes the safety factor 1.3 in the result of the SUPERFISH shunt impedance.

Table 7: Main DTL Parameters

Total Length	18.04	m
Cell Number	116	
Average Field	5.	MV/m
Structure Power	6.59	MW
Beam Power	3.20	MW
Average Power	70.5	kW
* Filling Time (Tf)	60.	micro sec
RF Pulse Width	120.	micro sec
Repetition Rate	60	Hz

$$\begin{aligned}
 * Tf &= 3(\text{Loaded } Q/(\pi * f_0)) \\
 &= 3(27000/(3.14 * 425\text{MHz}))
 \end{aligned}$$

2.3.3 RF Power Considerations

For our design, a suitable klystron is the VA-812E made by Varian. It is the same klystron designed for the PIGMI [15] [16] project at Los Alamos. Table 8 shows the specifications for it. One problem is the RF pulse width. We need a longer pulse width than the typical usage. There is the empirical law [17] between the pulse width and the peak power,

$$P_2 = P_1 * \sqrt{T_1/T_2},$$

where P_1 and T_1 are the peak power and the pulse width of the typical usage, and T_2 the width of this design. Then P_2 becomes about 8.16 MW. It comes out a little bit lower than the power required.

Table 8: Varian Klystron, Model VA-812E

Frequency range	400 to 450	MHz
Peak Output Power, min	20	MW
Gain	40	dB
Average Power	300	kW
Pulse Duration, RF	20	micro sec

Whether we make the whole DTL as one tank or a multi-tank is a matter for argument. There are some factors to be considered. First, it strongly depends on the available power source. If there is not enough power for a whole tank by one tube or klystron, we need to divide the tank so that each tank has an equal power dissipation. On this point, there is no problem as mentioned above.

Secondly, if we make the whole DTL as one tank, the total cell number in one tank becomes large and the mode separation between the operating mode (TM_{010}) and the nearest mode (TM_{011}) becomes small. According to the linear chain model, the mode separation between these two is

$$\Delta f = 4.3 * 10^{-2} \text{ MHz.}$$

In fact, to stabilize the electric field on the axis and to make a larger mode separation, we would also use post-couplers [18]. On the other hand, the frequency spread due to the quality factor Q is

$$\Delta f = 4.6 * 10^{-3} \text{ MHz.}$$

We have enough mode separation and there is no reason to divide the tank from this point of view.

Thirdly, if we divide the tank then we can use the intermediate energy beam by extracting it from the transport line between tanks. There is, in fact, the option to use a 15 MeV energy beam for isotope production (Appendix A).

Finally it is obvious that the fabrication and alignment methods are related to this issue.

We chose one tank at the first iteration. But the case of a multi-tank DTL is mentioned in Appendix A.

2.3.4 Beam Dynamics Calculations

The most fundamental parameters to be determined in the DTL are the transverse and longitudinal phase advance, μ_t and μ_l when we study the beam dynamics. In general, μ_t is a function of the strength of the quadrupoles, while μ_l is a function of the accelerating field gradient and the synchronous phase. We should determine

them first. Then the aperture, namely the bore radius, is calculated corresponding to the input beam emittance.

There are some interesting phenomena concerned with the dynamics of this DTL. First, compared with the conventional DTL, this design has a higher field gradient and a different relation between the longitudinal and transverse phase advance. We have to study the longitudinal and transverse coupling resonance more carefully.

Secondly, we consider that permanent magnet quadrupoles (PMQ) are the best choice because of their simplicity and adequate strength. However, a PMQ has a larger fringe field compared to an ordinary electromagnetic quadrupole. The coupling between the two transverse directions becomes an important issue.

Thirdly, the high brightness beam derived from the RFQ has a strong space charge force. This reduces the phase advance in both directions and causes emittance growth. The problem of how to handle this space-charge-dominated beam may be the main issue when we design a modern DTL.

Finally, alignment errors of the quadrupoles produce a distortion of the orbit. This effect plays a more important part in this 425 MHz DTL because the bore size is relatively small. We have to estimate this effect assuming some kind of error pattern rather than only a random distribution.

The purpose of the beam dynamics study is to determine the phase advances taking into account these considerations. Here we will give the preliminary results of the longitudinal-transverse (L-T) coupling and the space charge effects. A description of the beam dynamics codes used in this study is given in Appendix D.

We start with the following assumptions to study the beam dynamics. The quadrupole strength is determined to keep the phase advance μ_t constant. Here μ_t is

$$\cos \mu_t = 1 - (3 - 2\Lambda)/6 \cdot \Lambda^2 \Theta_0^4 - 2\Delta$$

where Λ is the packing factor of quadrupoles, Θ_0^2 is the quadrupole strength and Δ is the RF defocusing parameter. First, we will include the RF defocusing force but not space charge. We chose $\Lambda = 1/2$ and $\mu_t \simeq 75$ degrees. For the longitudinal direction, we

chose -30 degrees as a synchronous phase and 5 MeV as the field gradient.

If we take 5 mm as the bore radius, the 95 % normalized acceptance becomes,

$$\alpha_t = 1.1 \pi \text{ cm} \cdot \text{mrad},$$

$$\alpha_l = 9.0 \text{ deg} \cdot \text{MeV}.$$

The wave numbers of each direction are in the ranges

$$k_t = 22 \text{ to } 6 \quad 1/\text{m} \text{ (smoothed)},$$

$$k_l = 18 \text{ to } 2 \quad 1/\text{m}.$$

There are two coupling mechanisms between the longitudinal and transverse direction [19]. First, the RF defocusing force depends on the longitudinal phase. It produces a different transverse phase advance for each longitudinal initial phase. Secondly, an off-axis beam has a different energy gain due to the dependence of the accelerating field on the radial coordinate.

Here we only take note of the transverse equation for small oscillations

$$x'' + k_t x = \epsilon x \eta,$$

where $\eta = \phi - \phi_s$. If ϵ is small, then we can suppose x and η are described as

$$x = \cos k_t z, \quad \eta = \cos k_l z.$$

Substituting these into the above equation, we obtain

$$\begin{aligned} x'' + k_t x &= \epsilon \cos k_t z \cos k_l z \\ &= \frac{\epsilon}{2} [\cos(k_l + k_t)z + \cos(k_l - k_t)z]. \end{aligned}$$

From this, the resonance condition is,

$$2k_t - k_l = 0.$$

The wave number is a function of the field gradient, energy, synchronous phase and frequency,

$$k_t = \frac{\mu}{2\beta\lambda_0},$$

$$k_l = \left(\frac{-2\pi e E_0 \sin \phi_s}{m_0 c^2 \beta^3 \gamma^3 \lambda_0} \right)^{\frac{1}{2}},$$

where λ_0 is the RF wave length and μ is the phase advance per focusing unit. The typical numbers for a conventional 200 MHz DTL and this design are shown in Table 9.

Table 9: DTL Field Characteristics

	Conventional 200 MHz	This Design
Field	2.0 MV/m	5.0
Inj. Energy	0.75 MeV	2.3
Frequency	200 MHz	425
Synchr. Phi	-30 deg	-30

Using these numbers, we obtain the tune diagram as shown in Fig. 18, where $\nu_{t,l} = \mu_{t,l}/2\pi$. As for the resonance $2\nu_t - \nu_l = 0$, the operating line of this design is far from it.

Figure 19 shows that the relation between the field gradient and the emittance growth due to the L-T coupling using PARMILA. If the initial particles have no longitudinal spread, there is no emittance growth. We can see that if we take the field below 5 MV/m, there is no growth. The growth above this value occurs in the low energy section since the growth at the 10 MeV stage and the 66 MeV stage are almost same.

The tune diagram is shown in Fig. 20 for the case when the field is 10 MV/m and the transverse phase advance is about 40 degrees. If we increase the field gradient or decrease the transverse phase advance (by space charge for example), the operation line approaches the resonance.

We will initially suppose that the space charge force is described as a linear force. The transverse restoring force is represented by

$$K_t = K_q + K_{rf} + K_{sc},$$

where

$$K_q = B'/(B\rho),$$

$$K_{rf} = -\frac{\pi e E_0 T |\sin \phi_s|}{m_0 c^2 \lambda_0 \beta^3 \gamma^3},$$

$$K_{sc} = -\frac{3 Z_0 e I \lambda_0 (1 - f(p))}{8 \pi m_0 c^2 r^2 b \beta^2 \gamma^3},$$

where Z_0 is the impedance of free space, r is the transverse semi-axis, b is the longitudinal semi-axis, and

$$f(p) \sim 1/(3p), p = b/r.$$

In our case, these values are at injection

$$K_{rf}/K_q = 0.023,$$

$$K_{sc}/K_q = 0.180.$$

Space charge results in a reduction of 18 % in the phase advance.

Figure 21 shows the modulation of the envelope due to the space charge using TRACE3D. The matched line is first designed for no space charge. With 50 mA current the beam envelope is found to be two times larger. In TRACE3D there is no emittance growth because of the linear space charge force, but in an actual machine, space charge may cause the emittance to grow by a factor of four.

We use PARMILA to estimate the emittance growth due to space charge. Figure 22 shows the output beam profile at 0 mA and 50 mA. The input beam is distributed randomly in a four dimensional transverse hyperspace with random phase and energy spread within an ellipse. The beam is matched without space charge. At 50 mA, we can see the beam halo.

Figure 23 shows the relation between the beam current and the emittance growth factor. The other conditions are same as in Fig. 22. At 50 mA, both transverse emittances grow by a factor of two. There is a discrepancy in the growth between the x and y directions above 50 mA. This is not seen in the simulations using TRACE3D.

3 Conclusion

A 66 MeV proton linac for neutron therapy has been studied in this paper. A standard duoplasmatron has been assumed as the source for 30 keV protons. The entire LEPT, RFQ, and DTL have been conceptually designed using standard accelerator computer codes. All components of the design appear feasible with existing technology.

There are of course many issues that need to be addressed in any future detailed design. For a compact machine with high brightness beam, it appears that space charge effects are very important in determining the beam quality through the DTL. More detailed calculations and simulations of such effects should be done.

Acknowledgements

The authors would like to thank Dr. D. Young and Dr. A. Lennox for suggesting this design and for their great help. The authors would like to thank Dr. R. Noble for reading and making constructive criticisms of this paper. This work was done at Fermi National Accelerator Laboratory, and was supported in part by the Midwest Institute for Neutron Therapy at Fermilab. The authors would like to express their appreciation for very helpful discussions and contributions from the following individuals, Drs. C. Curtis, J. MacLachlan, F. Mills, A. Moretti, E. McCrory, L. Oleksiuk, C. Owen, and L. Teng.

References

- [1] A. J. Lennox, *Scenario for a Hospital Based Proton Linear Accelerator Neutron Therapy Facility*, Neutron Therapy Facility internal report, Fermilab, 1988.
- [2] A. Septier, *Focusing of Charged Particles*, Vol. 2, pp. 143-149, (Academic Press, New York, 1967).
- [3] F. Cole *et al.*, *Design and Application of a Proton Therapy Accelerator*, Proc. of the 1987 IEEE Particle Accel. Conf., p. 1985.
- [4] James Slater, Daniel W. Miller, and John O. Archaibeau, *Development of a Hospital-Based Proton Beam Treatment Center*, Int. J. Radiation Oncology Biol. Phys. Vol 14, pp. 761-775, (1988).
- [5] P. Spadtke, *AXCEL GSI*, GSI Report, GSI-83-9, 1983; *Computer Simulation of High Current DC Ion Beams*, Proc. of the 1984 Linear Accel. Conf., p. 356, GSI-84-11, N. Angert, ed.
- [6] R. H. Stokes *et al.*, *RF Quadrupole Beam Dynamics Design and Studies*, Proc. of the 1979 Linear Accel. Conf., p. 205, BNL Report 51134, R. L. Witkover, ed.
- [7] E. A. Wadlinger, *RFQ Scaling Law Implication and Example*, 1986 Linear Accel. Conf., p. 346, SLAC Report 303.
- [8] W. D. Kilpatrick, *Criterion for Vacuum Sparking Designed to Include Both RF and DC*, Rev. Sci. Inst. 28, p. 824, 1957.
- [9] R. J. Noble, *RF sparking rates per unit electrode area.*, unpublished, Fermilab, 1988; *Acceleration Gradient for the 400-MeV Linac Upgrade.*, TM-1448, Fermilab, 1987.
- [10] D. Raparia, *User guide to RFQSCOPE*, TAC Report, to be published.
- [11] H. Klean *et al.*, GSI Report, GSI-82-8, 1982.
- [12] R. Kazimi, Texas Accelerator Center, private communication.
- [13] Microwave Control Co. designed, *350 kW Amplifier System, Model No. S1150P350*, 1987.

- [14] O. R. Sander *et al.*, *Transverse Emittance of a 2.0 MeV RFQ Beam with High Brightness*, IEEE Trans. Nucl. Sci. NS-32, Part 1, p. 2588, (1985 Particle Accelerator Conf.).
- [15] Donald A. Swenson, *PIGMI: A Pion Generator for Medical Irradiations*, Los Alamos internal publication LAL-81-6, (1981).
- [16] T. J. Boyd *et al.*, *The PIGMI Technology*, Los Alamos internal publication LA-UR-80-3561, (1980).
- [17] A. Moretti, Fermilab, private communication.
- [18] S. Machida, *Study of the Alvarez Linac Stabilized with Post-Couplers*, KEK Report 85-11, 1985.
- [19] R. L. Gluckstern, *Linear Accelerators*, pp. 797-804, P. M. Lapostolle *et al.*, ed., (North-Holland Pub., Amsterdam, 1970).
- [20] T. P. Wangler, *Lumped Circuit Model of Four-Vane RFQ Resonator*, Proc. of the 1984 Linear Accel. Conf., p. 332, GSI-84-11, N. Angert, ed.
- [21] K. Halbach, *Physical and Optical Properties of REC Magnets*, Nucl. Instr. and Methods 187, pp. 109-117, 1981.

Appendices

A Some Clinical Options

A.1 Motivation

The original intent of this study was to reproduce, in a hospital setting, the therapy capabilities presently available at Fermilab's Neutron Therapy Facility. However, during the course of the study a few additional options were considered, though they were not examined carefully enough to determine whether they are really feasible from a financial and operational point of view. This section describes some preliminary work relative to these options and raises some still unanswered questions which must be addressed before settling on a definitive design. At present there is some interest in using epithermal neutrons to irradiate brain tumors. One possibility is to use 2.3 MeV protons on a lithium production target. That is the reason for specifying the 2.3 MeV RFQ. This study has found that it is possible to transport 2.3 MeV protons through the DTL without accelerating them, meaning that the DTL could deliver 66 MeV protons for ordinary therapy and 2.3 MeV protons for treating brain tumors. However, such a scheme would require electromagnetic rather than permanent quadrupoles. This would increase the complexity of the control system, would require the addition of power supplies for the quadrupoles, and would increase the power costs. It might be better to have a separate RFQ dedicated to treating brain tumors rather than complicating the design of the DTL to accommodate the lower energy protons. This question cannot be resolved until cost effectiveness issues are better understood.

Another desirable option is the capability of producing short-lived isotopes for medical procedures. Most medical radioisotopes are produced using 10 to 15 MeV protons from cyclotrons. This energy range could be achieved by degrading the 66 MeV beam or by building the DTL in four sections and accelerating beam only in the first section when isotopes are being produced. From an operational point of view the second method is more attractive, but a cost analysis must be done before a decision is made. It is

also possible to produce isotopes in the neutron beam. Some work must be done to determine the usefulness of these neutron-generated isotopes.

A.2 2.3 MeV Beam Transport through the DTL

As mentioned above, 2.3 MeV protons could be used for epithermal neutron production. For this purpose rf is turned off in the DTL, and it operates as a beam transport line. To use the DTL as a beam transport line we have to change the quadrupole strengths which are normally set for the DTL accelerating mode. Because of this we cannot use permanent magnet quadrupoles. One can show that to transport a 2.3 MeV beam with a constant phase advance per unit cell in the transverse direction through the DTL, the quadrupole strengths have to change (in the thin lens approximation) according to the formula

$$B'_n = B'_1 \frac{L_{q1} L_{c1}}{L_{qn} L_{cn}},$$

where B'_n and L_{qn} are the strength and the length of the n th quadrupole in the DTL, and L_{cn} is the length of the n th cell in the DTL.

Fig. 24 shows the 2.3 MeV beam evolution through the last ten cells in the DTL when the quadrupole strengths are set according to the formula given above.

A.3 Isotope Production

For the option of using a 15 - 20 MeV beam for isotope production, we designed the multi-tank option. If the output energy of the first tank is set to a value in the above range, we have to divide the linac into four tanks because of the equal power law. The power and the output energy of each tank are as follows.

Table A.1

Tank #1	2.30 - 18.97 MeV	2.511 MW
2	18.97 - 35.90	2.521
3	35.90 - 51.11	2.494
4	51.11 - 66.18	2.537

B RFQ Options

B.1 RFQ Structures

B.1.1 Four Vane

This is the very first structure mentioned for the RFQ. This structure has voltage stabilization problems. This problem can be solved by using VCR, RLC, DDR, and AHS coupling schemes. The power can be estimated as follows [20]. The electrostatic calculation shows that the capacitance per unit length is independent of radial aperture for a four vane structure with a circular tip whose radius of curvature is .75 times the circular aperture. The result obtained for such a circular vane tip is about 105 pico farad/meter. [12]

The power loss per unit length and quality factor of the structure are given by

$$P_l = 1.3 \cdot 10^{-3} (f C_t)^{3/2} V^2 = 160 \text{ kW/m},$$

$$Q = (\omega C_t V^2) / 2P_l = 11000,$$

where

$$\omega = 2\pi f,$$

$$f = 425 \text{ MHz}, V = 112.5 \text{ kV} \text{ and } r_0 = 0.3 \text{ cm}.$$

B.1.2 Four Rod

This structure was invented by the University of Frankfurt group. It does not have voltage stabilization problems, and it is very simple to fabricate. The power loss for this structure is estimated as follows [12]

$$P_i = R_s \left[\frac{2H + h}{w} + \frac{2h}{3 \text{ Rod Width}} \right] \frac{(\omega C_t LV)^2}{2n} = 210 \text{ kW},$$

and the quality factor Q is given by

$$Q = (\omega C_t V^2) / 2P_i = 8600,$$

where H, h, w are defined in Fig. 25 and

$$R_s = \sqrt{\omega \mu_0 \rho / 2},$$

$\mu_0 = 4\pi \cdot 10^{-7}$, $\rho = 0.17410^{-7}$,
 $n = 23, h = 4.34 \text{ cm}, w = 10 \text{ cm}, H = 10.7 \text{ cm}, V = 112.5 \text{ kV}$ and
 $L = 1 \text{ m}$.

B.1.3 TAC Design

This structure was recently developed at the Texas Accelerator Center. It is very simple to fabricate, has no voltage stabilization problems and has a lower power requirement than the four rod structure.

The power loss is estimated as follows [12]

$$P_i = R_s \left[\frac{1}{2\pi} \left(2 \ln \frac{R_2}{R_1} + \frac{h}{R_1} \right) + \frac{h}{3 \text{ Rod Width}} \right] \frac{(\omega C_t LV)^2}{2n} W = 200 \text{ kW},$$

and quality factor Q is given by

$$Q = (\omega C_t V^2) / 2P_i = 8800,$$

where h, R_1 and R_2 are defined in Fig. 4 and
 $n = 17, R_1 = 2.5 \text{ cm}, R_2 = 14.5 \text{ cm}$ and $h = L/n = 5.9 \text{ cm}$.

B.2 Matching to the DTL

B.2.1 Option 1

As we have mentioned in section 2.2.4, this option requires three quadrupoles and an rf gap (buncher). All three planes can be matched exactly for both zero current and full current. The quadrupole

strengths are approximately the same as in the first cell of the DTL. Table B.1 shows the quadrupole strengths, buncher parameters and the distances between them. Figure 26 shows the result of TRACE3D for this matching.

B.2.2 Option 2

This option requires a PRMS and a half length quadrupole. Figure 27 shows the vane shape in the PRMS. The quadrupole strength is 288 Tesla/m. Figure 28 shows the TRACE3D output for this option.

Table B.1

1st Quadrupole	
Strength	288 T/m
Length	2.4 cm
2nd Quadrupole	
Strength	288 T/m
Length	2.4 cm
RF Gap	
EoTL	.125 MV
Phase	-90. deg

C SUPERFISH Design Code

We have examined the computational accuracy and mesh size dependence of SUPERFISH. First we compared the analytical and the computed value for a pillbox cavity in Fig. 29, taking the mesh size as a parameter. Table C.1 shows that there is no mesh size dependence for the resonant frequency and the difference from the analytical value is only 0.002 %.

Table C.1

Mesh Size	Frequency
0.08 cm	546.39 MHz
0.10	546.39
0.20	546.39
0.50	546.40
0.80	546.40
Analytical Value	546.38

Secondly, the same mesh size dependence was examined for the shape of the DTL as shown in Fig. 30. The DTL shape is so complicated that we cannot calculate the value analytically. Figure 31 shows that by decreasing the mesh size, the resonant frequency does converge. As a result if we take less than 0.25 cm as the mesh size, the resonant frequency is determined within about 1 MHz (0.2 %).

Finally, we found a relation between the accuracy of the resonant frequency and the effective shunt impedance as shown Fig. 32. From this figure, we see that if we determine the frequency with an error of about 1 MHz, we can obtain the effective shunt impedance with an error of 0.2 %. For the effective use of SUPERFISH, we took 0.25 cm as a maximum mesh size and permitted a frequency error of 1 MHz in the calculations.

D Beam Dynamics Codes

We used the beam simulation codes PARMILA and TRACE3D. PARMILA is a multi-particle tracking code, while TRACE3D is a transformation code for the beam envelope. In both cases, each cell of the DTL is represented by a half-quadrupole, drift space, RF impulse, drift space and a half-quadrupole. We make some comparisons between these two codes in the following.

D.1 Example of GENLIN Output

The parameters of the structure were determined by using the subroutine GENLIN in PARMILA for both codes. Table D.1 is an example of GENLIN output.

In this table, the maximum quadrupole field is 28.9 kG/cm, which seems quite high. But this is the result when we take the packing factor as 1/2. By making the magnet length equal the drift tube length, we can reduce the magnet strength. Specifically the ratio of the drift tube length to the cell length at the lowest β is about 0.8, therefore the magnet length can be lengthened by 1.6 times. This almost corresponds to the reduction of 0.6 in the magnet strength. In this case, the magnet strength becomes 18.0 kG/cm, which is a moderate value.

D.2 Comparison of the Basic Lattice

For the transverse direction, both programs assume a linear lattice. Each transverse transfer matrix is described by a 2×2 matrix independently. There is no nonlinear term. For the longitudinal direction, TRACE3D assumes small oscillations and the potential is described as

$$U = \sin \phi_s \cdot |\Delta\phi|^2 .$$

where $\Delta\phi = \phi - \phi_s$, ϕ_s is a synchronous phase and ϕ the phase of each particle. On the other hand, PARMILA assumes the exact cosine form of the field and the potential is

$$U = \sin(\phi_s + \Delta\phi) - \Delta\phi \cdot \cos \phi_s .$$

The results of these two programs for the case of no space charge and no alignment error agree as shown in Fig. 33, except for a slight difference in the longitudinal direction due to the potentials.

D.3 Treatment of Space Charge

The TRACE3D code assumes a linear force arising from a uniform charge distribution of a three dimensional ellipsoid. There is no emittance growth independent of beam current. In PARMILA, the beam is separated into rings and the electric field induced by each

ring is calculated. Then the force on each beam is estimated by the integration over these fields.

D.4 Longitudinal-Transverse Coupling

In PARMILA, the radial dependence of the accelerating field is approximated by the expansion of the modified Bessel function to second order. Also the RF defocusing force is calculated for individual particles.

D.5 Permanent Magnet Quadrupoles

In TRACE3D, there is a subroutine that deals with the permanent magnet quadrupole in addition to the ordinary hard-edge electromagnetic quadrupole. It assumes a certain functional form for the fringe field [21] and includes the focusing by this field.

Table D.1. Output of GEMIN

CELL NUMBER INITIAL	KINETIC ENERGY	BETA	LENGTH	T	TP	S	SP	QUAD LENGTH	QUAD GRADIENT	EZERO MV/M	PHIS	TOTAL LENGTH
1	2.3000	0.0699	5.0142	0.8016	0.0584	0.4575	0.0523	2.4650	28.8752	5.0000	-30.00	0.000
2	2.4740	0.0725	5.1972	0.8061	0.0553	0.4539	0.0525	2.5562	-27.7984	5.0000	-30.00	5.014
3	2.6554	0.0751	5.3811	0.8106	0.0542	0.4502	0.0526	2.6479	26.7986	5.0000	-30.00	10.211
4	2.8443	0.0777	5.5660	0.8152	0.0531	0.4466	0.0528	2.7409	-26.8509	5.0000	-30.00	15.592
5	3.0408	0.0803	5.7518	0.8197	0.0520	0.4429	0.0529	2.8326	24.8708	5.0000	-30.00	21.158
6	3.2450	0.0830	5.9380	0.8243	0.0508	0.4392	0.0531	2.9257	-24.1451	5.0000	-30.00	26.910
7	3.4569	0.0856	6.1263	0.8290	0.0497	0.4355	0.0532	3.0193	23.3688	5.0000	-30.00	32.849
8	3.6768	0.0883	6.3149	0.8336	0.0485	0.4318	0.0534	3.1133	-22.6378	5.0000	-30.00	38.975
9	3.9048	0.0909	6.5045	0.8383	0.0474	0.4280	0.0536	3.2077	21.9482	5.0000	-30.00	45.290
10	4.1409	0.0936	6.6949	0.8430	0.0462	0.4242	0.0539	3.3027	-21.2966	5.0000	-30.00	51.795
11	4.3853	0.0961	6.8864	0.8477	0.0451	0.4205	0.0540	3.3981	20.6801	5.0000	-30.00	58.490
12	4.6389	0.0987	7.0786	0.8522	0.0440	0.4174	0.0541	3.4939	-20.0958	5.0000	-30.00	65.376
13	4.8992	0.1018	7.2711	0.8568	0.0439	0.4147	0.0540	3.5902	19.5413	5.0000	-30.00	72.454
14	5.1675	0.1045	7.4636	0.8614	0.0439	0.4118	0.0542	3.6826	-19.0131	5.0000	-30.00	79.726
15	5.4430	0.1072	7.6558	0.8656	0.0438	0.4182	0.0543	3.7877	18.5134	5.0000	-30.00	87.189
16	5.7257	0.1100	7.8479	0.8697	0.0438	0.4188	0.0544	3.8787	-18.0398	5.0000	-30.00	94.845
17	6.0155	0.1127	8.0400	0.8739	0.0437	0.4189	0.0546	3.9747	17.5905	5.0000	-30.00	102.693
18	6.3125	0.1154	8.2319	0.8783	0.0437	0.4193	0.0547	4.0707	-17.1637	5.0000	-30.00	110.733
19	6.6167	0.1181	8.4230	0.8826	0.0436	0.4197	0.0548	4.1666	16.7577	5.0000	-30.00	118.965
20	6.9280	0.1209	8.6153	0.8868	0.0436	0.4201	0.0549	4.2625	-16.3710	5.0000	-30.00	127.388
21	7.2465	0.1236	8.8088	0.8911	0.0435	0.4205	0.0550	4.3582	16.0024	5.0000	-30.00	136.004
22	7.5722	0.1263	9.0033	0.8954	0.0435	0.4208	0.0551	4.4540	-15.6505	5.0000	-30.00	144.810
23	7.9050	0.1290	9.1993	0.8997	0.0434	0.4212	0.0552	4.5498	15.3144	5.0000	-30.00	153.809
24	8.2450	0.1317	9.3963	0.9040	0.0434	0.4216	0.0553	4.6456	-14.9930	5.0000	-30.00	162.998
25	8.5921	0.1344	9.5912	0.9083	0.0433	0.4220	0.0554	4.7406	14.6864	5.0000	-30.00	172.378
26	8.9464	0.1371	9.7872	0.9126	0.0433	0.4224	0.0554	4.8360	-14.3900	5.0000	-30.00	181.949
27	9.3079	0.1398	9.9819	0.9169	0.0432	0.4227	0.0555	4.9313	14.1088	5.0000	-30.00	191.711
28	9.6764	0.1425	10.1762	0.9212	0.0432	0.4231	0.0556	5.0266	-13.8308	5.0000	-30.00	201.664
29	10.0522	0.1452	10.3719	0.9255	0.0431	0.4235	0.0557	5.1217	13.5764	5.0000	-30.00	211.807
30	10.4351	0.1479	10.5683	0.9297	0.0431	0.4239	0.0559	5.2167	-13.3261	5.0000	-30.00	222.140
31	10.8261	0.1506	10.7650	0.9340	0.0430	0.4242	0.0560	5.3117	13.0853	5.0000	-30.00	232.663
32	11.2289	0.1533	10.9626	0.9383	0.0430	0.4246	0.0561	5.4061	-12.8564	5.0000	-30.00	243.378
33	11.6394	0.1561	11.1619	0.9426	0.0430	0.4249	0.0562	5.5003	12.6293	5.0000	-30.00	254.285
34	12.0568	0.1588	11.3626	0.9469	0.0430	0.4252	0.0563	5.5943	-12.4108	5.0000	-30.00	265.385
35	12.4808	0.1615	11.5642	0.9512	0.0430	0.4255	0.0564	5.6883	12.1908	5.0000	-30.00	276.677
36	12.9114	0.1642	11.7672	0.9555	0.0430	0.4258	0.0565	5.7815	-11.9982	5.0000	-30.00	288.159
37	13.3488	0.1669	11.9719	0.9597	0.0430	0.4261	0.0566	5.8749	11.8031	5.0000	-30.00	299.832
38	13.7927	0.1696	12.1782	0.9640	0.0430	0.4264	0.0567	5.9687	-11.6149	5.0000	-30.00	311.690
39	14.2431	0.1723	12.3863	0.9683	0.0430	0.4267	0.0568	6.0626	11.4334	5.0000	-30.00	323.749
40	14.7002	0.1750	12.5960	0.9726	0.0430	0.4270	0.0569	6.1566	-11.2582	5.0000	-30.00	335.991
41	15.1637	0.1776	12.8072	0.9769	0.0430	0.4273	0.0570	6.2506	11.0889	5.0000	-30.00	348.422
42	15.6336	0.1803	13.0199	0.9812	0.0430	0.4276	0.0571	6.3446	-10.9254	5.0000	-30.00	361.042
43	16.1099	0.1830	13.2342	0.9855	0.0430	0.4279	0.0572	6.4386	10.7672	5.0000	-30.00	373.849
44	16.5929	0.1856	13.4499	0.9897	0.0430	0.4282	0.0573	6.5326	-10.6141	5.0000	-30.00	386.843
45	17.0820	0.1883	13.6672	0.9940	0.0430	0.4285	0.0574	6.6266	10.4660	5.0000	-30.00	400.024
46	17.5775	0.1910	13.8860	0.9983	0.0430	0.4288	0.0575	6.7206	-10.3226	5.0000	-30.00	413.391
47	18.0794	0.1936	14.1062	1.0026	0.0430	0.4291	0.0576	6.8146	10.1830	5.0000	-30.00	426.944
48	18.5874	0.1961	14.3279	1.0069	0.0430	0.4294	0.0577	6.9086	-10.0489	5.0000	-30.00	440.682
49	19.1017	0.1988	14.5512	1.0112	0.0430	0.4297	0.0578	7.0026	9.9183	5.0000	-30.00	454.665
50	19.6222	0.2014	14.7760	1.0155	0.0430	0.4300	0.0579	7.0966	-9.7916	5.0000	-30.00	468.712
51	20.1485	0.2040	15.0022	1.0198	0.0430	0.4303	0.0580	7.1906	9.6685	5.0000	-30.00	483.002
52	21.2186	0.2066	15.2299	1.0241	0.0430	0.4306	0.0581	7.2846	-9.5491	5.0000	-30.00	497.476
53	22.3315	0.2091	15.4592	1.0284	0.0430	0.4309	0.0582	7.3786	9.4333	5.0000	-30.00	512.132
54	22.8664	0.2117	15.6900	1.0327	0.0430	0.4312	0.0583	7.4726	-9.3207	5.0000	-30.00	526.970
55	23.4209	0.2143	15.9222	1.0370	0.0430	0.4315	0.0584	7.5666	9.2114	5.0000	-30.00	541.988
56	23.9929	0.2168	16.1563	1.0413	0.0430	0.4318	0.0585	7.6606	-9.1052	5.0000	-30.00	557.188
57	24.5829	0.2194	16.3919	1.0456	0.0430	0.4321	0.0586	7.7546	9.0020	5.0000	-30.00	572.567
58	25.1899	0.2219	16.6288	1.0499	0.0430	0.4324	0.0587	7.8486	-8.9016	5.0000	-30.00	588.126
59	25.8144	0.2244	16.8670	1.0542	0.0430	0.4327	0.0588	7.9426	8.8039	5.0000	-30.00	603.862
60	26.4564	0.2269	17.1072	1.0585	0.0430	0.4330	0.0589	8.0366	-8.7089	5.0000	-30.00	619.777
61	26.7237	0.2295	17.3499	1.0628	0.0430	0.4333	0.0590	8.1306	8.6104	5.0000	-30.00	635.869
62	27.0922	0.2320	17.5942	1.0671	0.0430	0.4336	0.0591	8.2246	-8.5263	5.0000	-30.00	652.138

62	20.0040	0.2345	16.4450	0.8329	0.0503	0.4631	0.0000	0.2095	8.4385	5.0000	-30.00	668.583
63	27.5029	0.2369	16.6205	0.8314	0.0507	0.4651	0.0001	8.3570	-8.3531	5.0000	-30.00	685.204
64	28.1065	0.2394	16.7963	0.8300	0.0511	0.4671	0.0003	8.4443	0.2698	5.0000	-30.00	701.999
65	28.7153	0.2419	16.9695	0.8285	0.0515	0.4692	0.0004	8.5313	-8.1800	5.0000	-30.00	718.968
66	29.3293	0.2443	17.1430	0.8271	0.0519	0.4712	0.0006	8.6179	0.1894	5.0000	-30.00	736.111
67	29.9484	0.2468	17.3159	0.8257	0.0523	0.4732	0.0007	8.7042	-8.0321	5.0000	-30.00	753.427
68	30.5726	0.2492	17.4882	0.8243	0.0527	0.4752	0.0009	8.7903	7.9568	5.0000	-30.00	770.916
69	31.2023	0.2517	17.6638	0.8507	0.0451	0.4424	0.0590	8.8769	-7.70854	5.0000	-30.00	788.579
70	31.8388	0.2542	17.8405	0.8485	0.0457	0.4454	0.0592	8.9670	7.9111	5.0000	-30.00	806.420
71	32.4830	0.2567	18.0164	0.8464	0.0464	0.4484	0.0594	9.0548	-7.7307	5.0000	-30.00	824.436
72	33.1359	0.2592	18.1915	0.8441	0.0470	0.4514	0.0596	9.1422	7.6681	5.0000	-30.00	842.628
73	33.7974	0.2617	18.3658	0.8419	0.0476	0.4544	0.0598	9.2292	-7.5993	5.0000	-30.00	860.994
74	34.4675	0.2641	18.5393	0.8397	0.0483	0.4573	0.0600	9.3157	7.5321	5.0000	-30.00	879.533
75	35.1461	0.2666	18.7119	0.8375	0.0489	0.4603	0.0602	9.4019	-7.4666	5.0000	-30.00	898.245
76	35.8331	0.2690	18.8838	0.8353	0.0495	0.4632	0.0604	9.4877	7.4026	5.0000	-30.00	917.129
77	36.5284	0.2714	19.0548	0.8332	0.0501	0.4661	0.0606	9.5730	-7.3402	5.0000	-30.00	936.183
78	37.2317	0.2738	19.2251	0.8310	0.0508	0.4690	0.0608	9.6580	7.2793	5.0000	-30.00	955.408
79	37.9425	0.2762	19.3945	0.8289	0.0514	0.4719	0.0610	9.7425	-7.2197	5.0000	-30.00	974.803
80	38.6609	0.2786	19.5632	0.8268	0.0520	0.4748	0.0612	9.8267	7.1616	5.0000	-30.00	994.366
81	39.3865	0.2810	19.7310	0.8247	0.0526	0.4777	0.0613	9.9104	-7.1047	5.0000	-30.00	1014.097
82	40.1192	0.2834	19.8981	0.8226	0.0532	0.4806	0.0615	9.9938	7.0492	5.0000	-30.00	1033.995
83	40.8591	0.2857	20.0644	0.8205	0.0538	0.4834	0.0617	10.0768	-6.9949	5.0000	-30.00	1054.060
84	41.6064	0.2880	20.2299	0.8184	0.0544	0.4862	0.0619	10.1594	6.9418	5.0000	-30.00	1074.289
85	42.3611	0.2904	20.3946	0.8163	0.0550	0.4890	0.0621	10.2415	-6.8899	5.0000	-30.00	1094.684
86	43.1232	0.2927	20.5585	0.8142	0.0556	0.4918	0.0623	10.3233	6.8391	5.0000	-30.00	1115.243
87	43.8927	0.2950	20.7217	0.8122	0.0562	0.4946	0.0626	10.4048	-6.7894	5.0000	-30.00	1135.904
88	44.6686	0.2973	20.8840	0.8101	0.0568	0.4974	0.0628	10.4858	6.7408	5.0000	-30.00	1156.848
89	45.4509	0.2996	21.0457	0.8081	0.0574	0.5002	0.0630	10.5664	-6.6932	5.0000	-30.00	1177.894
90	46.2396	0.3019	21.2065	0.8061	0.0580	0.5029	0.0633	10.6467	6.6467	5.0000	-30.00	1199.100
91	47.0347	0.3044	21.3666	0.8040	0.0586	0.5053	0.0631	10.7265	-6.6011	5.0000	-30.00	1220.467
92	47.8361	0.3069	21.5258	0.8019	0.0592	0.5077	0.0632	10.8050	6.5564	5.0000	-30.00	1241.993
93	48.6438	0.3096	21.6843	0.7995	0.0598	0.5100	0.0633	10.8851	-6.5127	5.0000	-30.00	1263.677
94	49.4578	0.3109	21.8421	0.7975	0.0603	0.5124	0.0634	10.9638	6.4699	5.0000	-30.00	1285.519
95	50.2781	0.3131	21.9990	0.7954	0.0609	0.5147	0.0635	11.0421	-6.4280	5.0000	-30.00	1307.518
96	51.1047	0.3153	22.1551	0.7933	0.0615	0.5171	0.0636	11.1200	6.3869	5.0000	-30.00	1329.673
97	51.9376	0.3175	22.3105	0.7912	0.0621	0.5194	0.0637	11.1976	-6.3460	5.0000	-30.00	1351.984
98	52.7769	0.3197	22.4651	0.7891	0.0627	0.5217	0.0637	11.2746	6.3072	5.0000	-30.00	1374.449
99	53.6224	0.3218	22.6190	0.7871	0.0632	0.5240	0.0638	11.3514	-6.2685	5.0000	-30.00	1397.068
100	54.4739	0.3240	22.7721	0.7850	0.0638	0.5262	0.0639	11.4278	6.2306	5.0000	-30.00	1419.840
101	55.3314	0.3262	22.9244	0.7829	0.0644	0.5285	0.0640	11.5038	-6.1934	5.0000	-30.00	1442.765
102	56.1949	0.3283	23.0760	0.7809	0.0649	0.5308	0.0641	11.5794	6.1570	5.0000	-30.00	1465.841
103	57.0644	0.3304	23.2269	0.7789	0.0655	0.5330	0.0642	11.6547	-6.1212	5.0000	-30.00	1489.067
104	57.9399	0.3326	23.3769	0.7768	0.0661	0.5353	0.0642	11.7290	6.0862	5.0000	-30.00	1512.444
105	58.8214	0.3347	23.5263	0.7748	0.0666	0.5375	0.0643	11.8041	-6.0518	5.0000	-30.00	1535.971
106	59.7089	0.3369	23.6749	0.7728	0.0672	0.5397	0.0644	11.8782	6.0180	5.0000	-30.00	1559.646
107	60.6024	0.3390	23.8228	0.7708	0.0677	0.5419	0.0645	11.9520	-5.9849	5.0000	-30.00	1583.460
108	61.5019	0.3410	23.9699	0.7689	0.0683	0.5441	0.0646	12.0254	5.9524	5.0000	-30.00	1607.438
109	62.4074	0.3430	24.1163	0.7669	0.0688	0.5463	0.0647	12.0984	-5.9205	5.0000	-30.00	1631.555
110	63.3189	0.3451	24.2620	0.7649	0.0694	0.5484	0.0647	12.1711	5.8892	5.0000	-30.00	1655.816
111	64.2364	0.3471	24.4069	0.7630	0.0699	0.5506	0.0648	12.2434	-5.8584	5.0000	-30.00	1680.223
112	65.1599	0.3492	24.5512	0.7610	0.0704	0.5527	0.0649	12.3154	5.8283	5.0000	-30.00	1704.776
113	66.0894	0.3512	24.6947	0.7591	0.0710	0.5549	0.0650	12.3870	-5.7986	5.0000	-30.00	1729.469
114	67.0249	0.3532	24.8376	0.7572	0.0715	0.5570	0.0651	12.4582	5.7695	5.0000	-30.00	1754.307
115	68.0664	0.3552	24.9790	0.7553	0.0720	0.5591	0.0652	12.5291	-5.7409	5.0000	-30.00	1779.286
116	69.1139	0.3572	25.1210	0.7534	0.0726	0.5612	0.0652	12.5997	5.7128	5.0000	-30.00	1804.408

Figure Captions

- Fig. 1A Particle trajectories through the LEBT.
- Fig. 1B Phase space plot at 22 cm.
- Fig. 2 Beam size, phase and energy profiles.
- Fig. 3A Input beam emittances in x-xp, y-yp and phi-w planes.
- Fig. 3B Output beam emittances in x-xp, y-yp and phi-w planes.
- Fig. 4 Schematic of the circular-inductor four rod RFQ basic module developed at TAC.
- Fig. 5 The vane shape in the PRMS (with no modulation) for option 3.
- Fig. 6 Matched phase spaces and the beam envelope at zero current for option 3.
- Fig. 7 Measured RFQ transmissions for several values of voltage (absolute transmissions are renormalized to 100%).
- Fig. 8 Matched phase spaces and the beam envelope at full current for option 3.
- Fig. 9 Dependence of the effective shunt impedance on the tank radius at different velocities.
- Fig. 10 Dependence of the effective shunt impedance on the drift tube radius at $\beta = 0.065$.
- Fig. 11 Relation between the drift tube radius and the maximum field gradient at $\beta = 0.065$.

- Fig. 12 Dependence of the effective shunt impedance on the stem radius at $\beta = 0.065$.
- Fig. 13 Dependence of the effective shunt impedance on the nose corner radius at different velocities.
- Fig. 14 Relation between the nose corner radius and the maximum field gradient at different velocities.
- Fig. 15 One cell of the DTL at $\beta = 0.065, 0.150, 0.250$.
- Fig. 16 Optimized effective shunt impedance with the velocity.
- Fig. 17 Variation of the maximum field gradient with the velocity.
- Fig. 18 Tune diagram of the longitudinal and transverse motion in the case of the typical 200 MHz and 425 MHz DTL.
- Fig. 19 Emittance growth due to the longitudinal-transverse coupling.
- Fig. 20 Tune diagram of the DTL with high field gradient and small transverse phase advance.
- Fig. 21 Envelope of the first 20 cells in the DTL in the case of 0 mA and 50 mA.
- Fig. 22 Output beam emittance of the DTL in the case of 0 mA and 50 mA.
- Fig. 23 Emittance growth due to the space charge effects.
- Fig. 24 2.3 MeV beam evolution through the last ten cells in the DTL.
- Fig. 25 Schematic of the twin-inductor four-rod RFQ

basic module.

- Fig. 26 Matched phase spaces and the beam envelope at zero current for option 1.
- Fig. 27 The vane shape in the PRMS (with no modulation) for option 2.
- Fig. 28 Matched phase spaces and the beam envelope at full current for option 2.
- Fig. 29 Pillbox cavity used to compare the analytical and computational resonant frequency.
- Fig. 30 Low β DTL cell used to measure the mesh dependence in SUPERFISH.
- Fig. 31 Mesh size dependence of the resonant frequency in SUPERFISH.
- Fig. 32 Fluctuation of the effective shunt impedance due to the accuracy of the resonant frequency.
- Fig. 33 Comparison of the TRACE3D and PARMILA without space charge.

$I = 50 \text{ mA}$

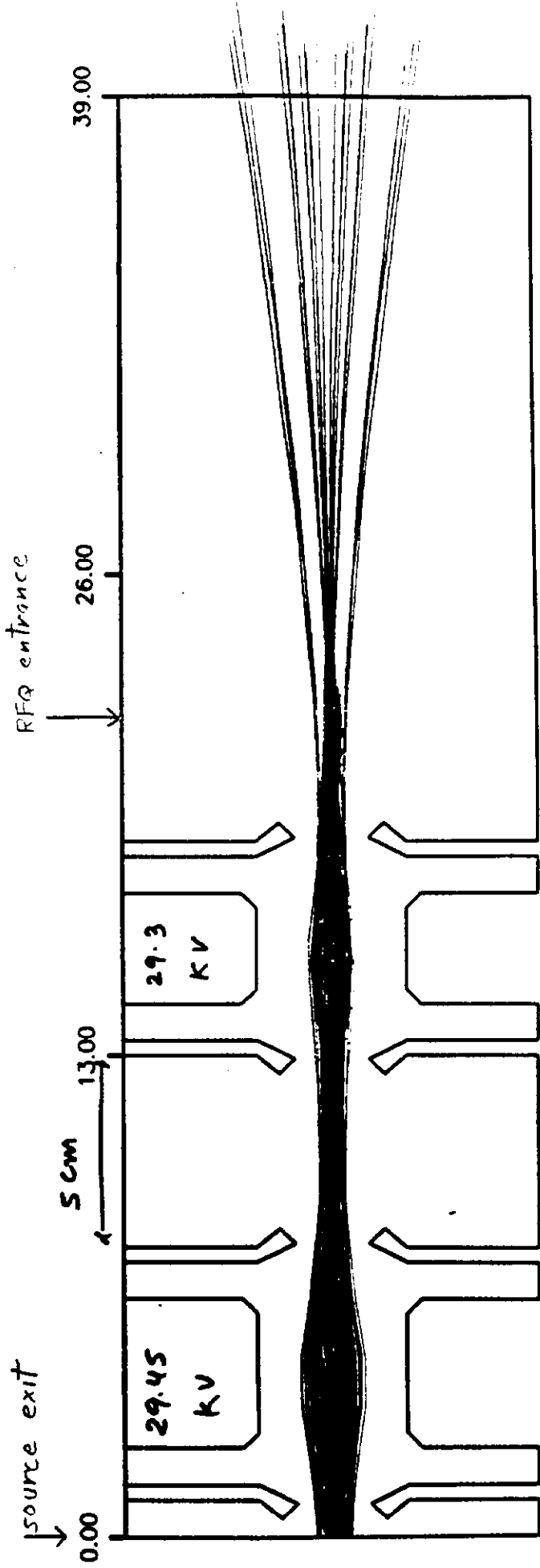
$\epsilon_N = .5 \text{ mm mrad}$

$\alpha = -3$

$\beta = .5 \text{ m}$

Fig. 1 A

AXCEL-TAM VERSION 85 TRAJEKTORIENPLOT RUN NUMBER 23.

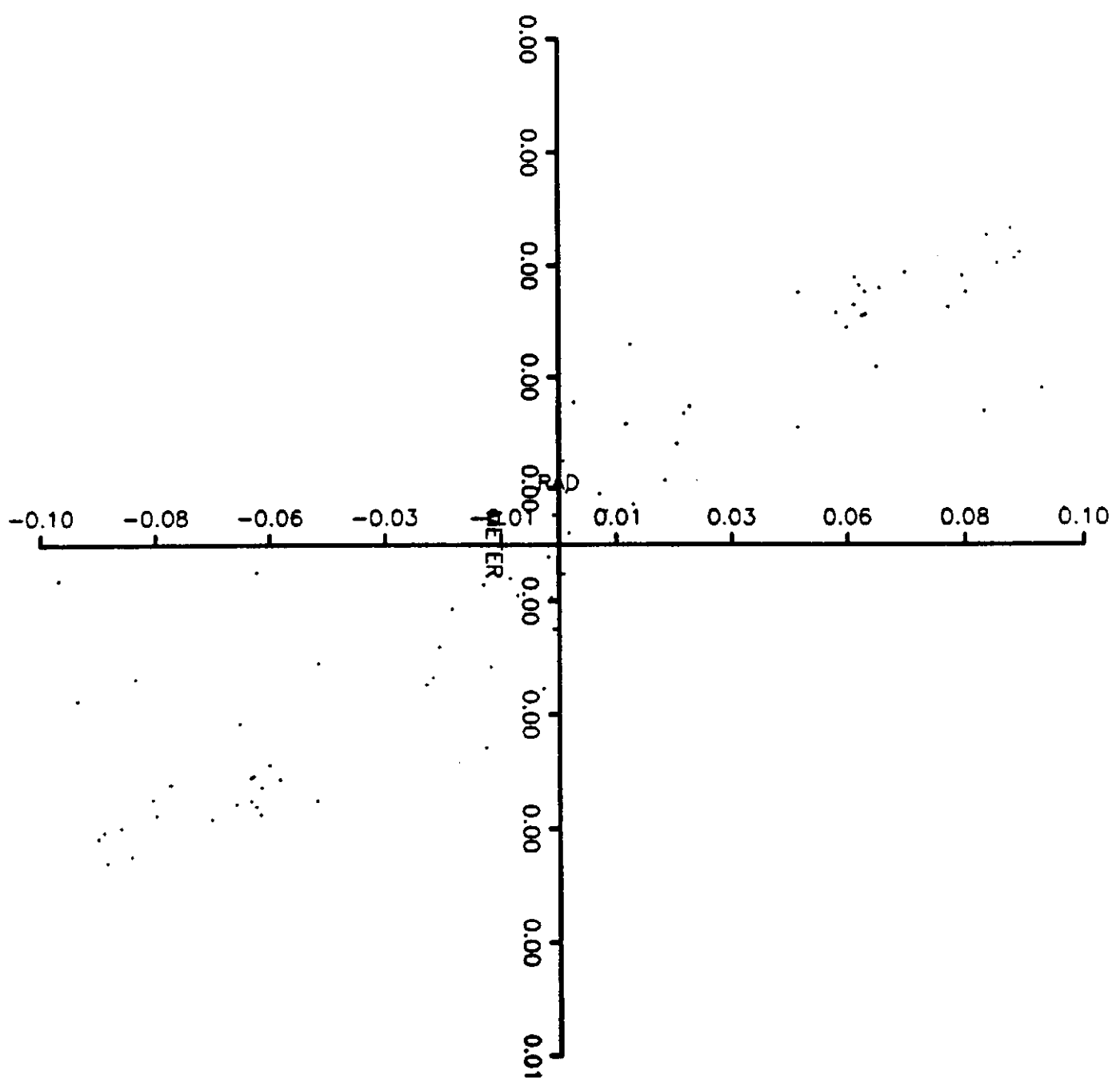


COMMENT: COMENT(1)

CYCLE: 10. PLOT: 10. DATE: 17-JUN-88

ZEIT: 10:12:34

19. 19. MA
PROZENT DER TRAJEKTORIEN



AXCEL-TAM VERSION 85 DATE: 21-JUN-88 ZEIT: 09:23:15
RADIALE EMITTANZ COMMENT: COMENT(1)
RUN NUMBER 52.CYCLE : 10. PLOT: 20.

Fig. 1 B

BCFJA158CEN1>+CFJA158CEN1>+JUC)KJA178CEN1>+BQJ<JA158CEN1>+I

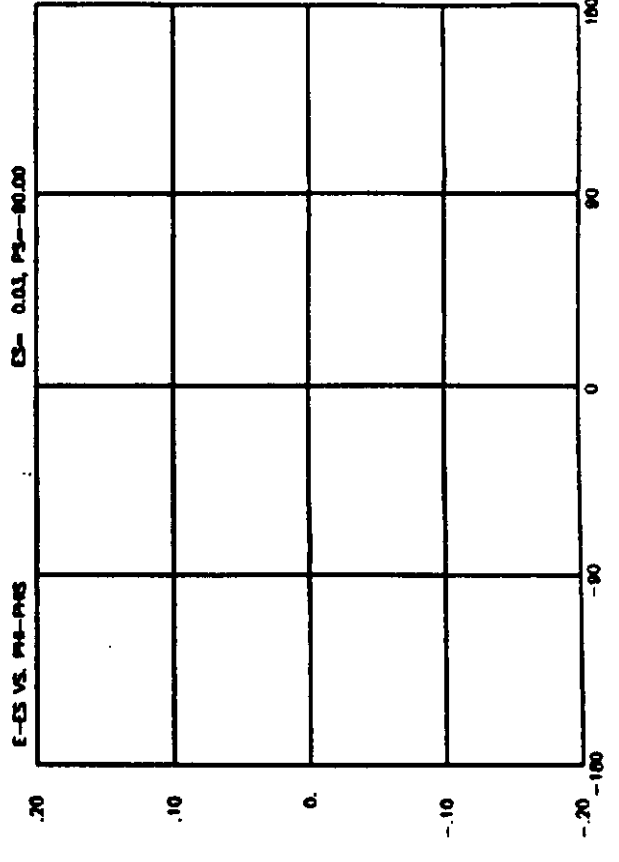
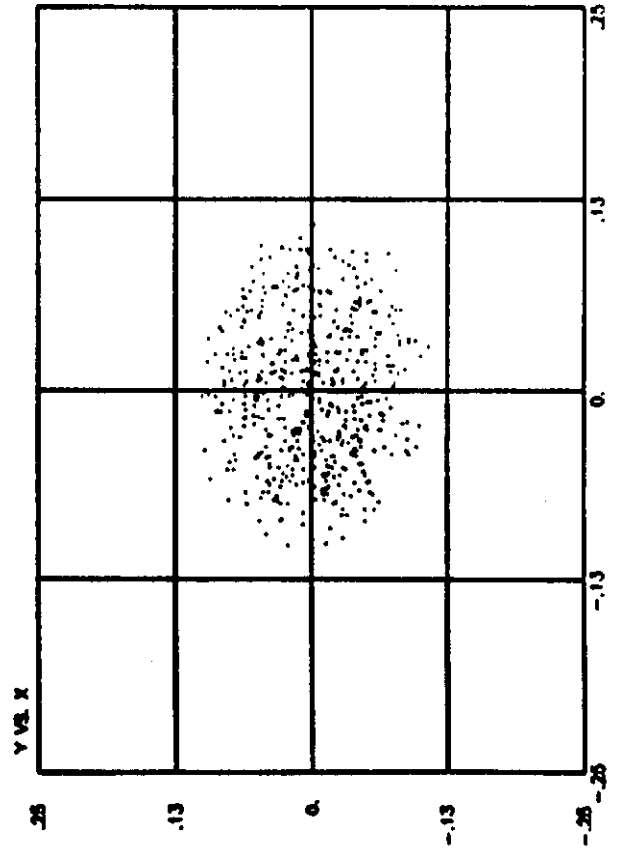
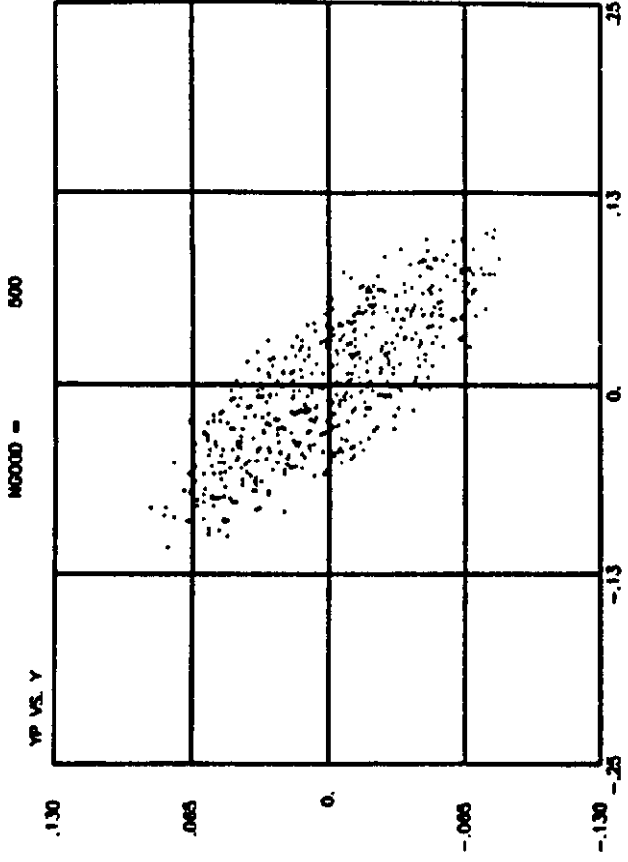
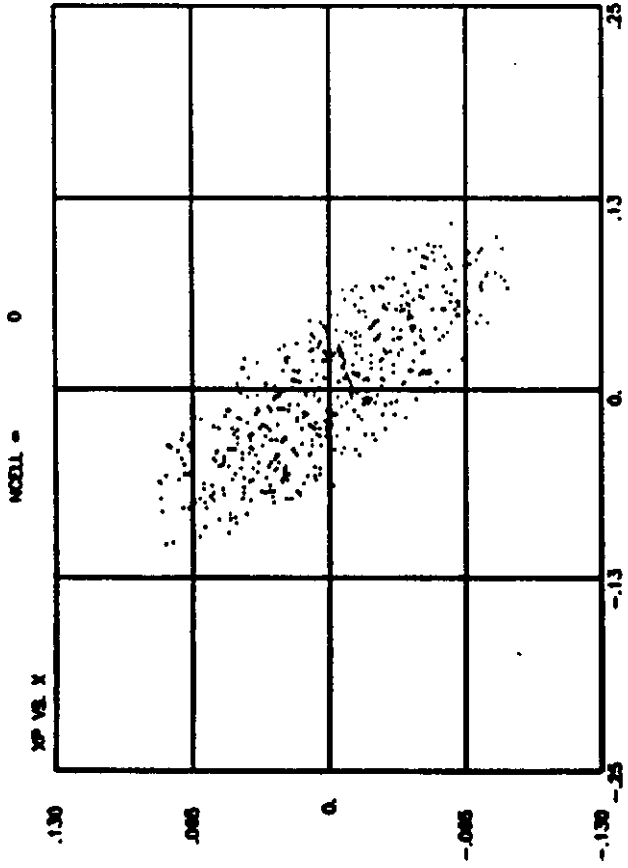
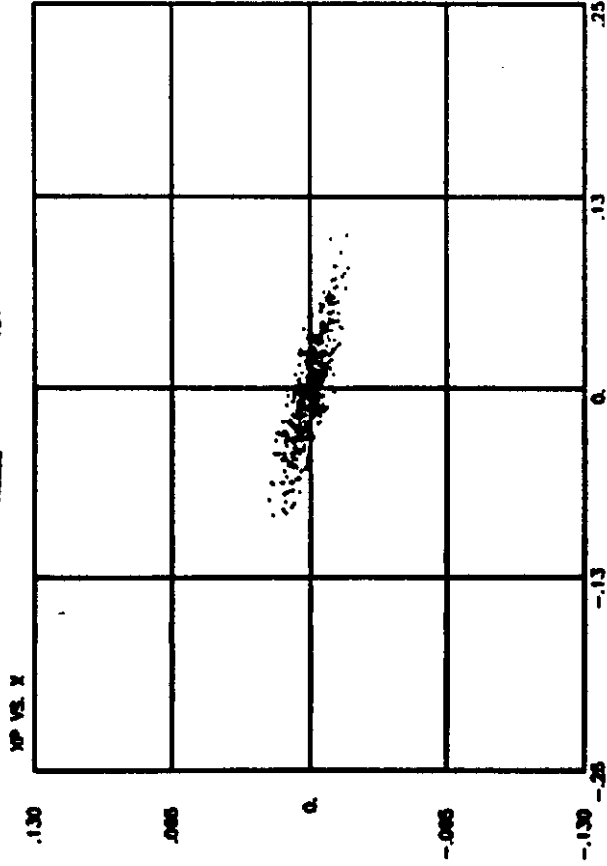


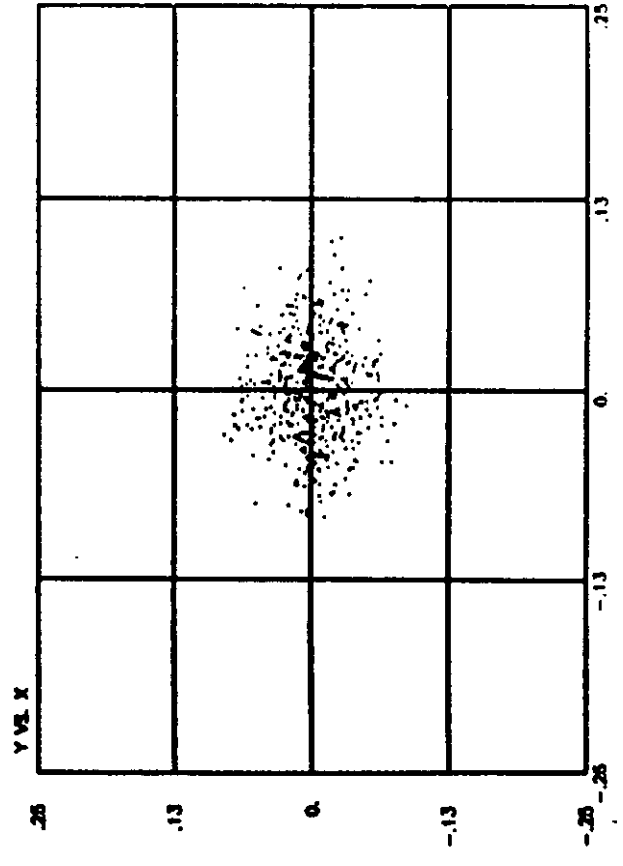
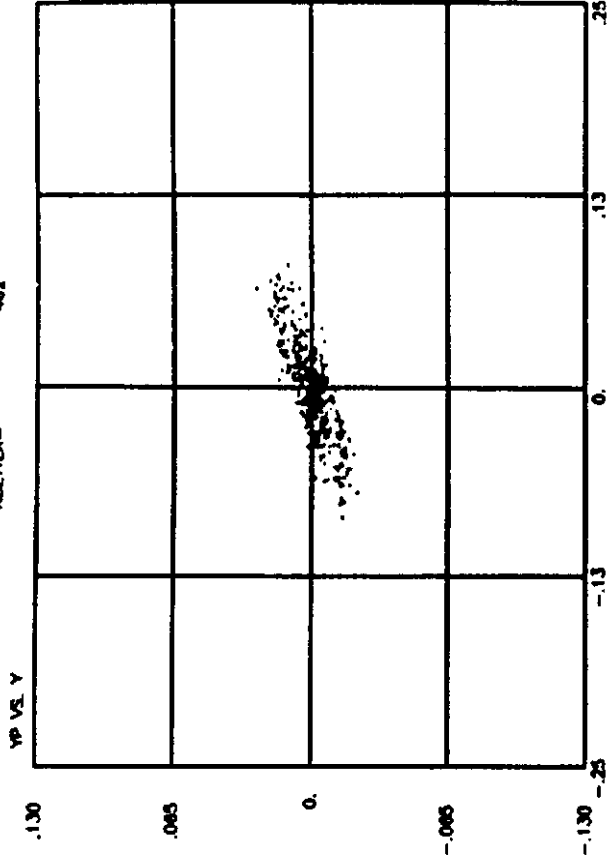
Fig. 3A

BCJAU18R:SA11>+1-CR1A118R:SA11>+1UC)CA117R:SA11>+1E1CUA118R:SA11>+1

MODEL = 131



MODEL = 462



ES = 2.31, PS = -28.22

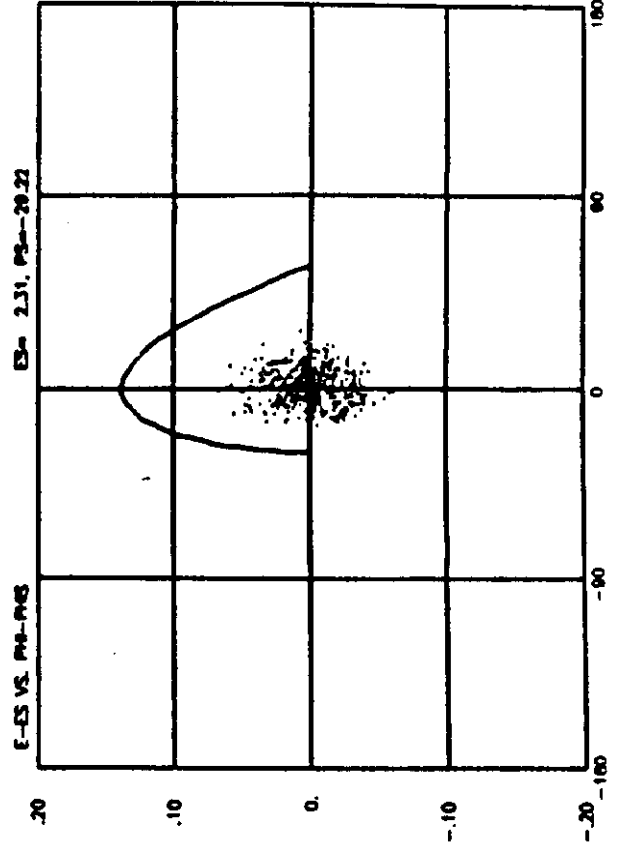


Fig. 3B

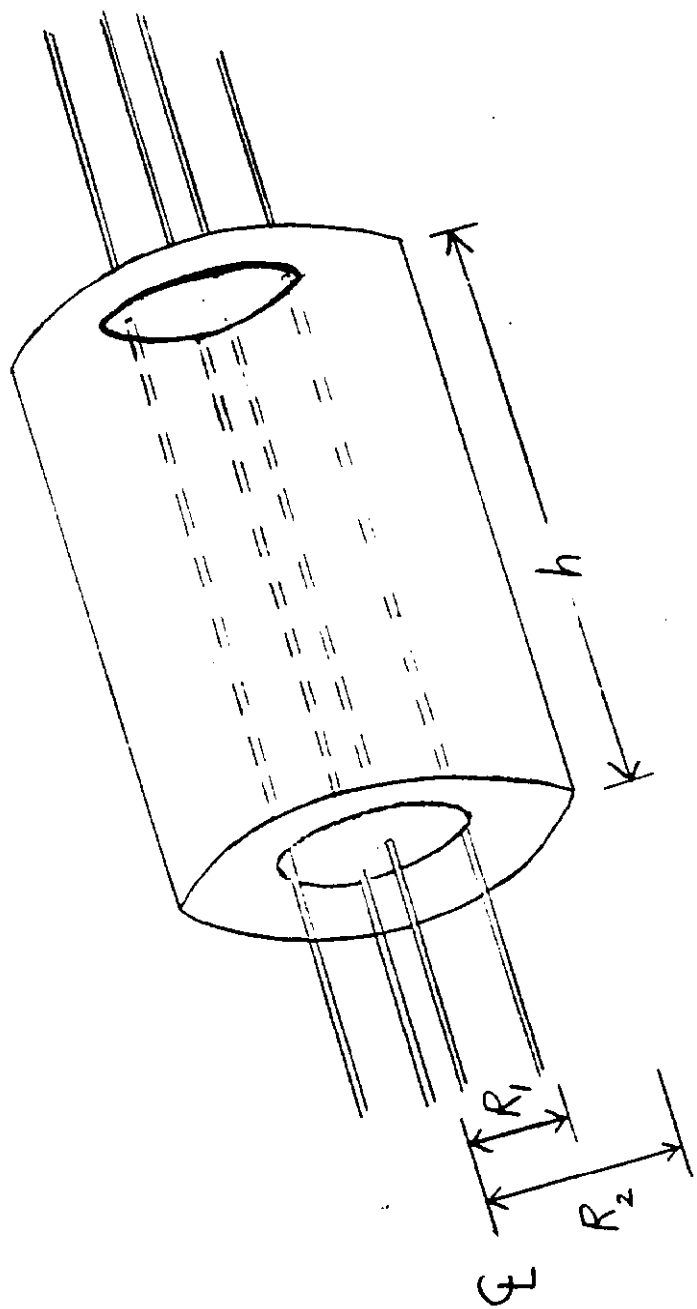


Fig. 4

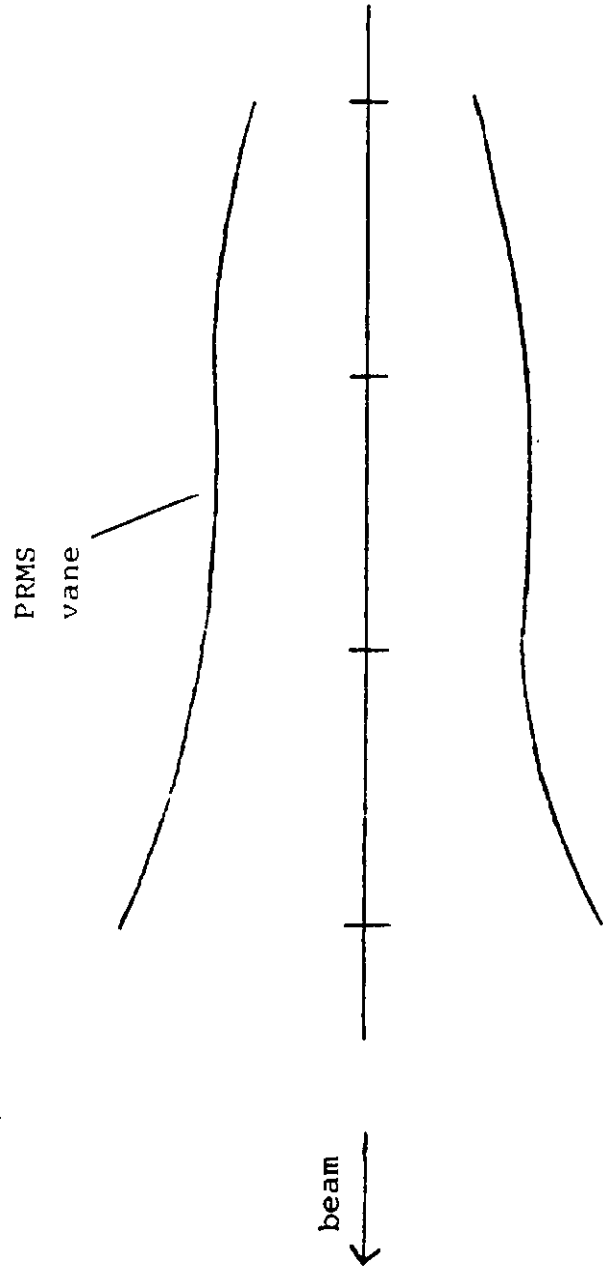
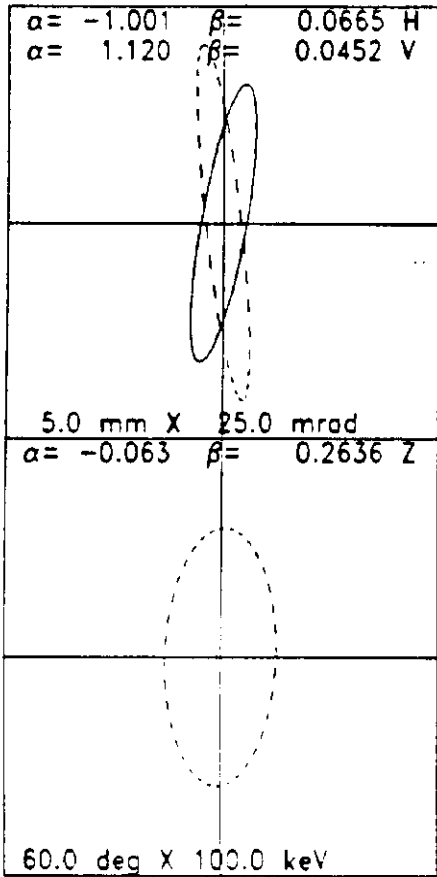


Fig. 5

Trace-3D Calculations

17-JUN-88 09:02:48



Beam Current= 0.0
 EMIT1= 8.57 8.57 900.00
 EMIT0= 8.57 8.57 900.00
 W= 2.300 2.300

Phi= 146.4 deg, W= 2.300 MeV
 DP= 23.2 deg, DW= 58.543 keV
 DZ= 3.18 mm
 DP/P= 12.74 mrad
 EMITZ= 26.83 pi mm-mrad

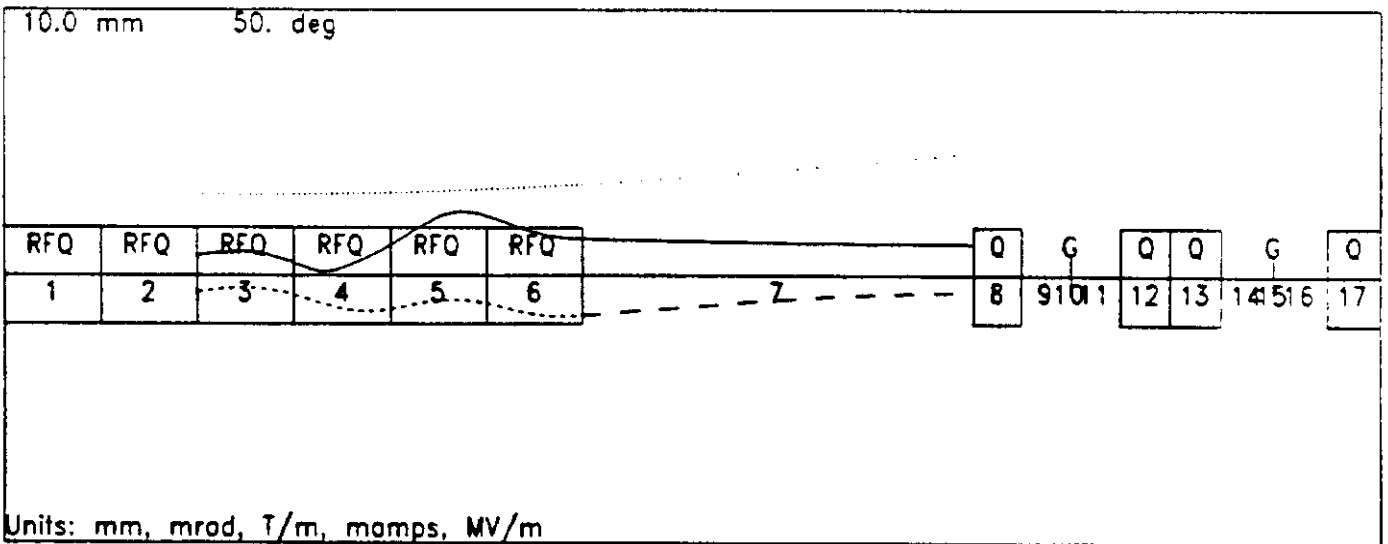
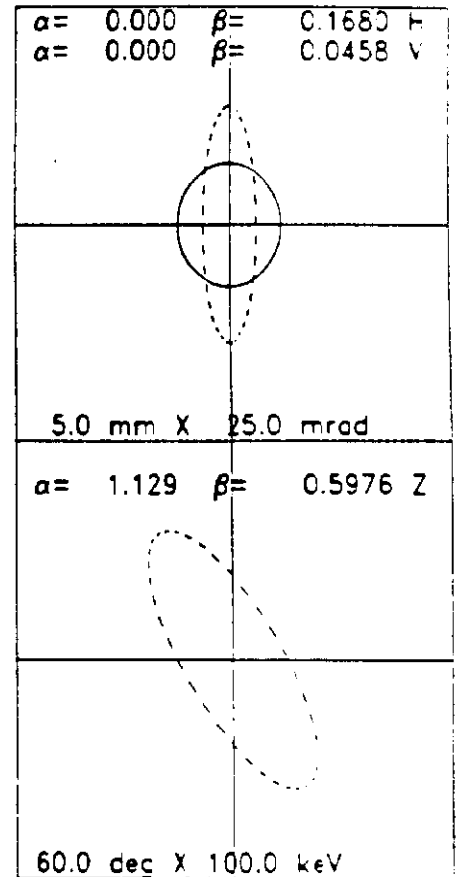
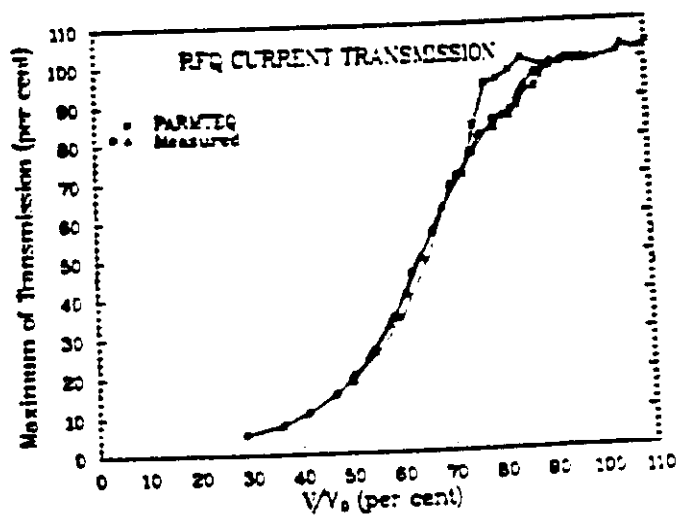
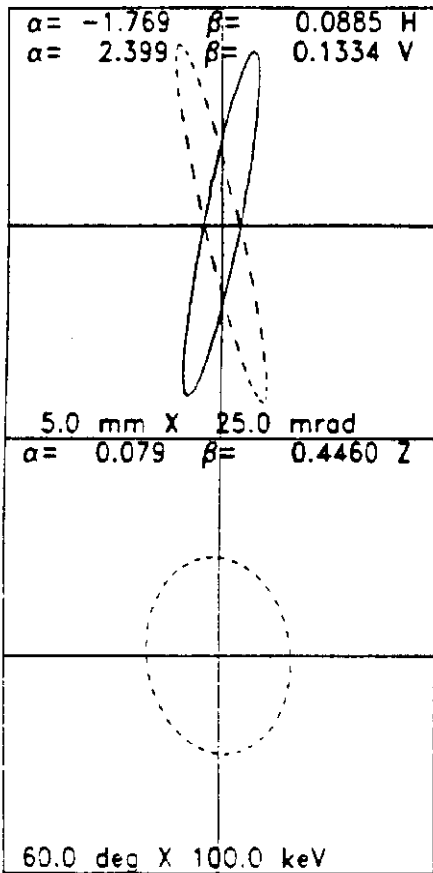


Fig. 6



Measured RFQ transmissions for several values of input mismatch (absolute transmissions are renormalized to 100%).

Fig. 7



Beam Current= 50.0
 EMITI= 8.57 8.57 900.00
 EMITG= 8.57 8.57 900.00
 W= 2.300 2.300
 Phi= 146.4 deg, W= 2.300 MeV
 DP= 29.7 deg, DW= 63.326 keV
 DZ= 4.06 mm
 DP/P= 13.78 mrad
 EMITZ= 26.83 pi mm-mrad

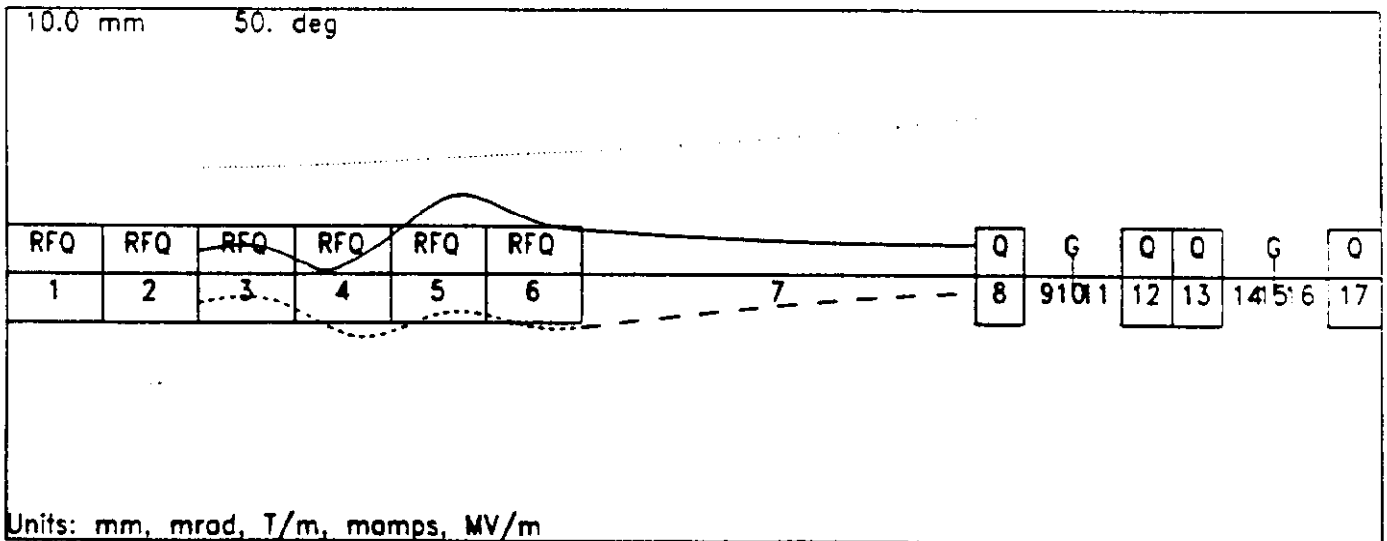
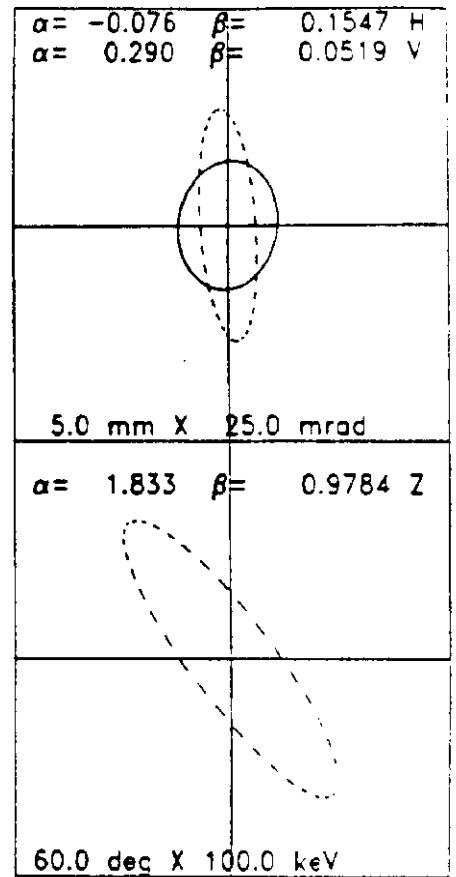


Fig. 8

Fig. 9

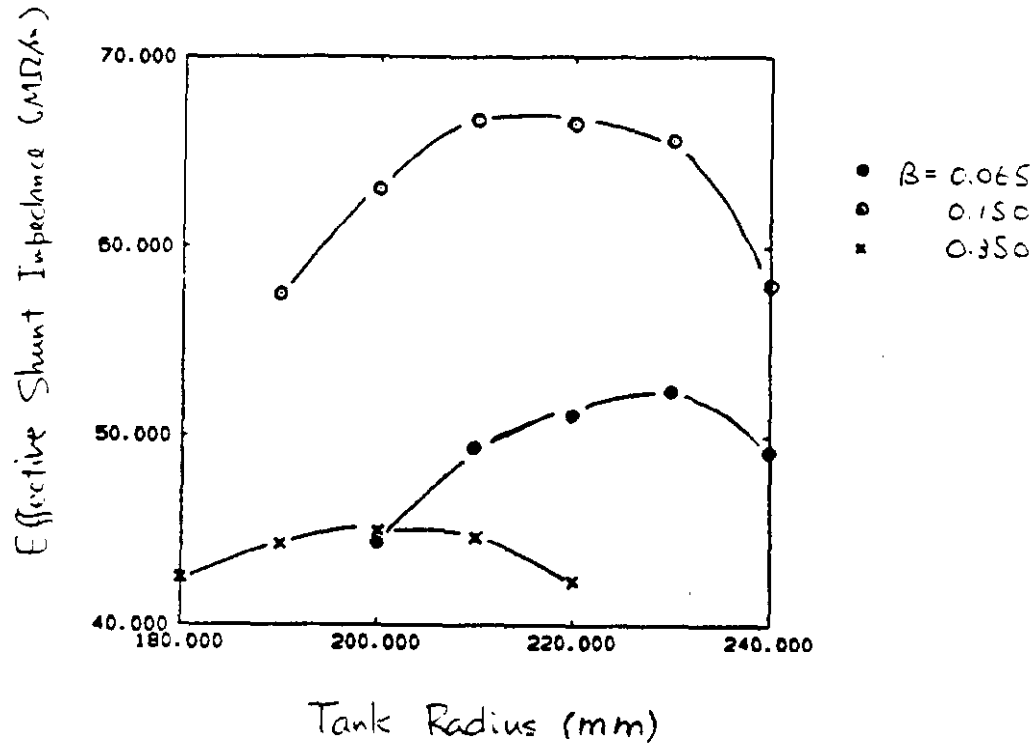


Fig. 10

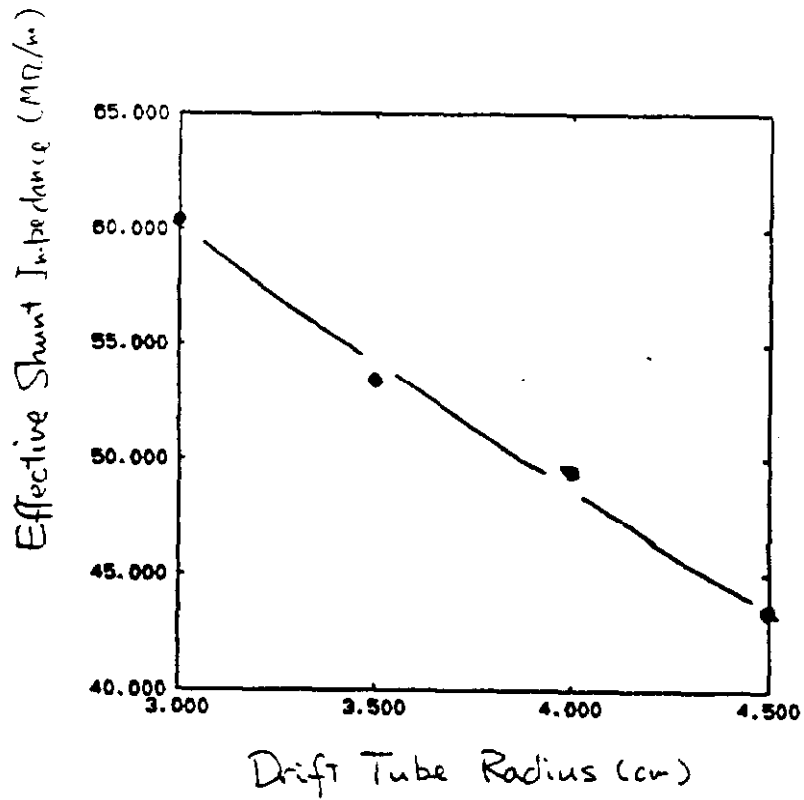


Fig. 11

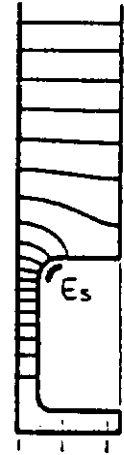
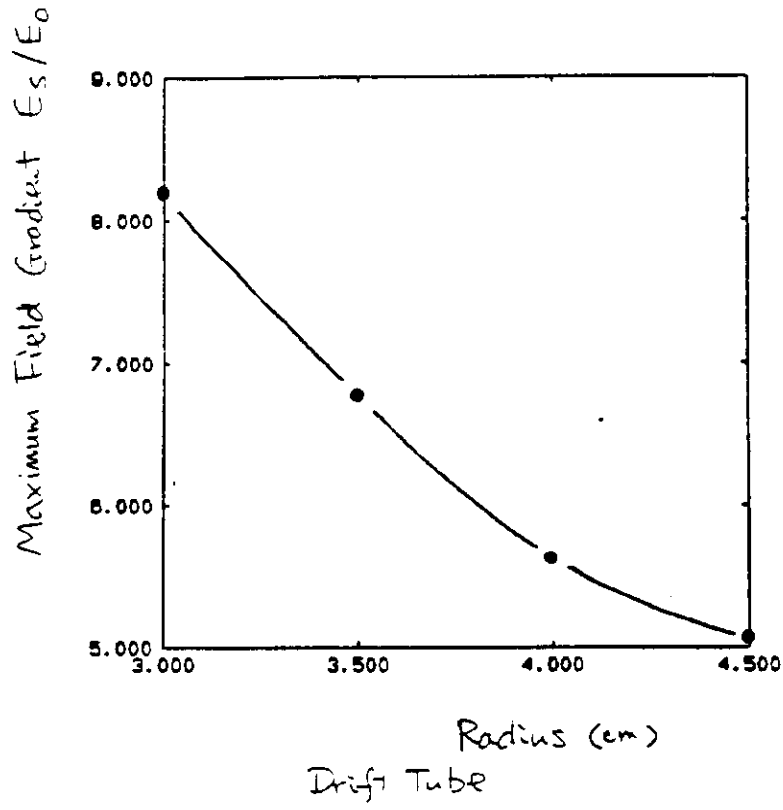


Fig. 12

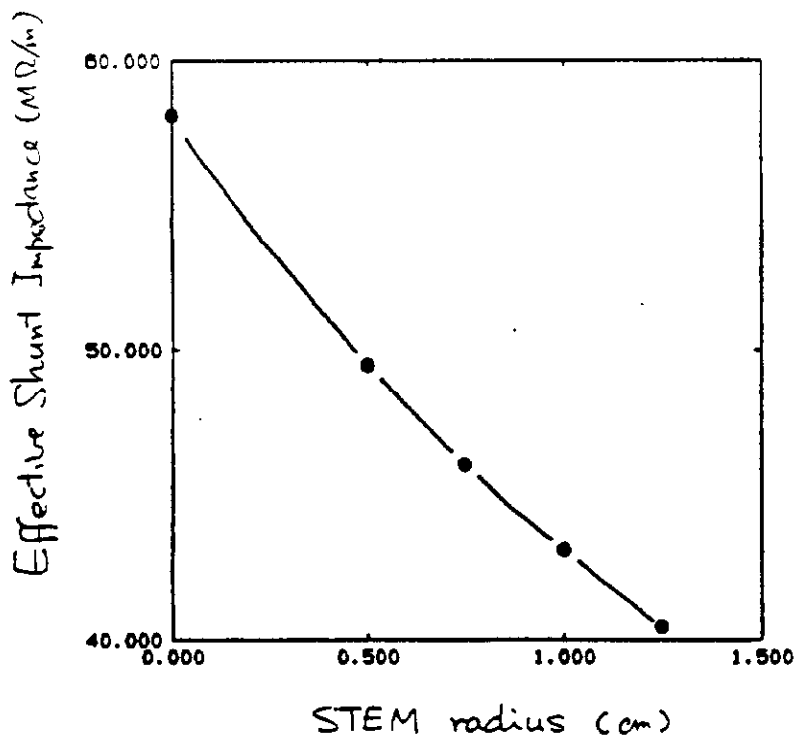


Fig. 13

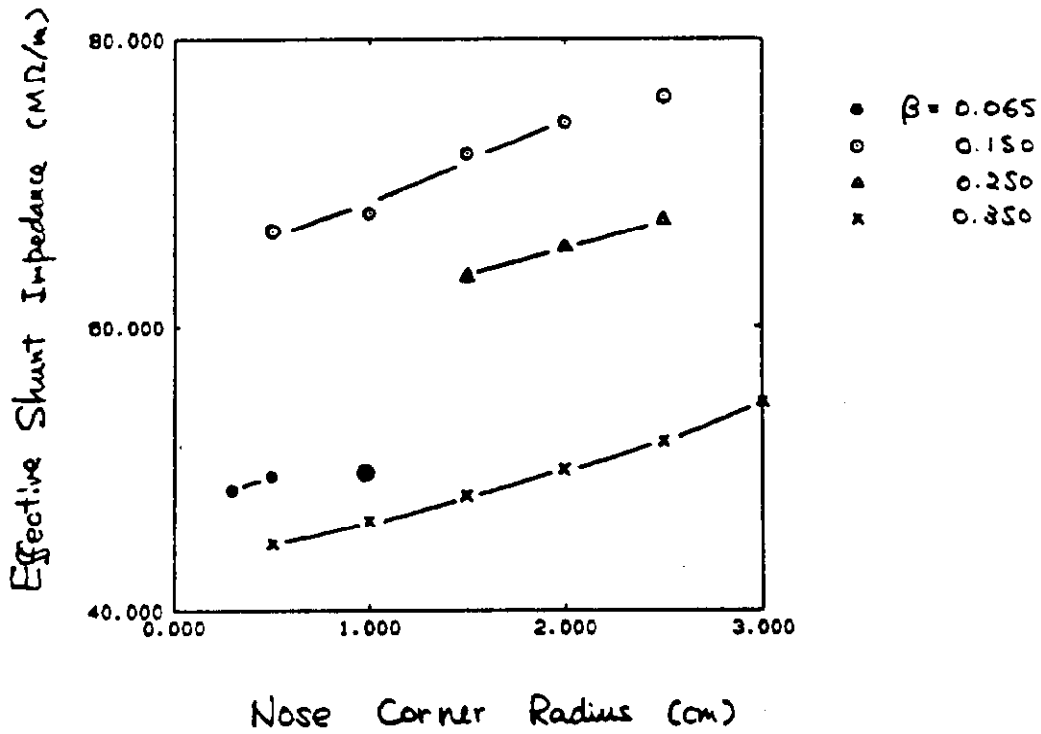
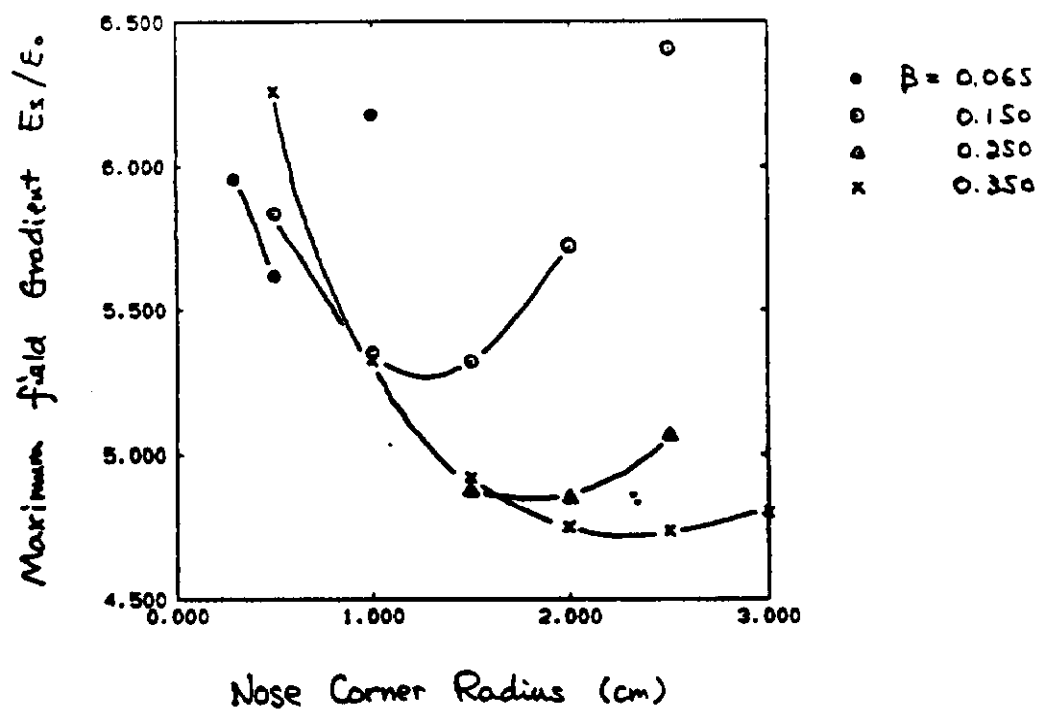
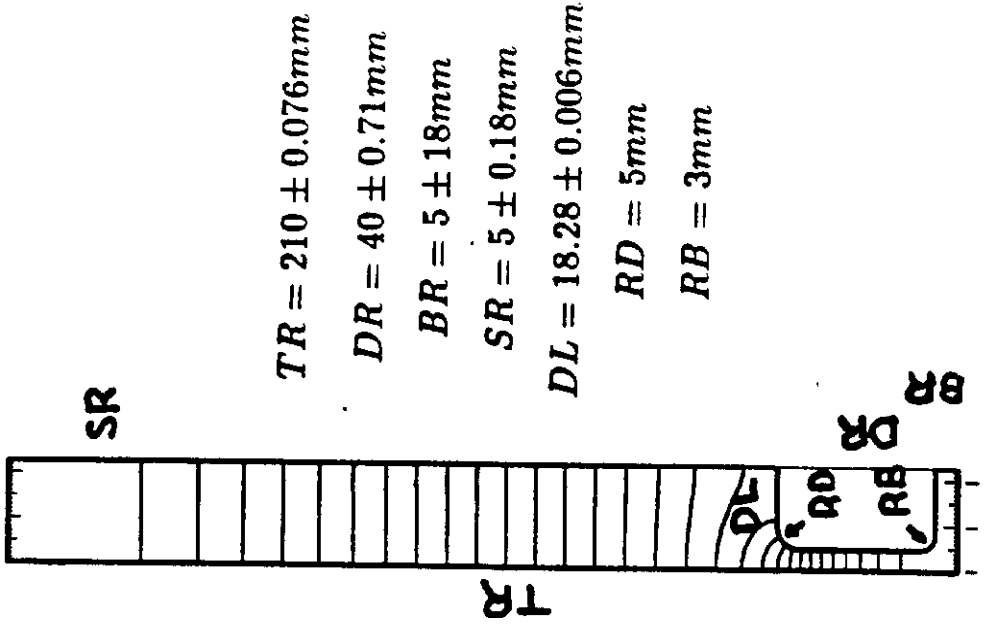
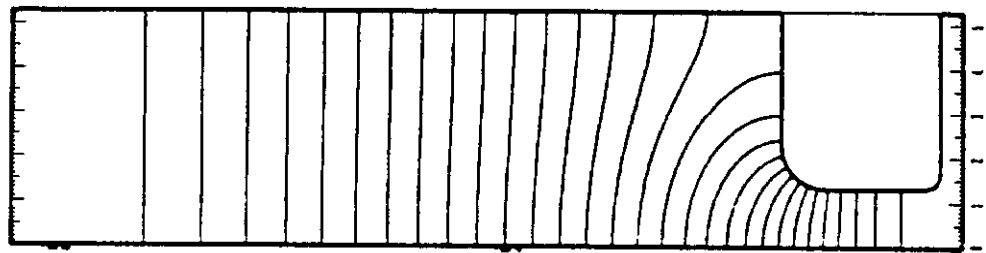
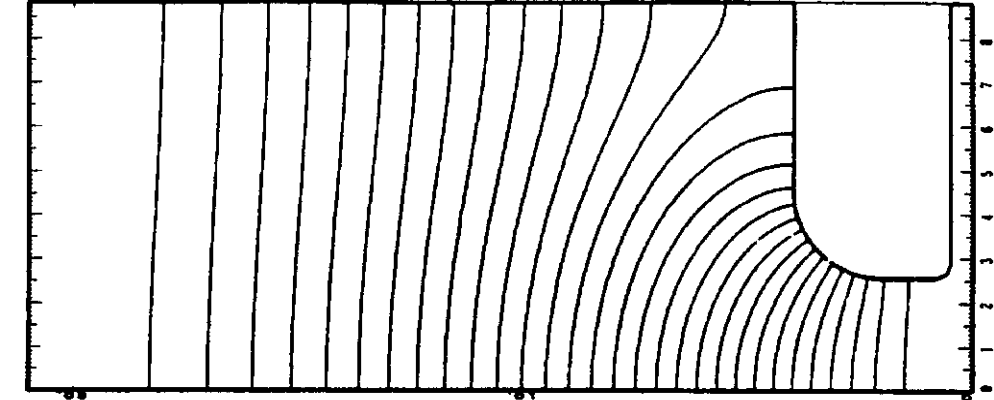


Fig. 14





$TR = 210 \pm 0.076mm$

$DR = 40 \pm 0.71mm$

$BR = 5 \pm 18mm$

$SR = 5 \pm 0.18mm$

$DL = 18.28 \pm 0.006mm$

$RD = 5mm$

$RB = 3mm$

Fig. 15

Fig. 16

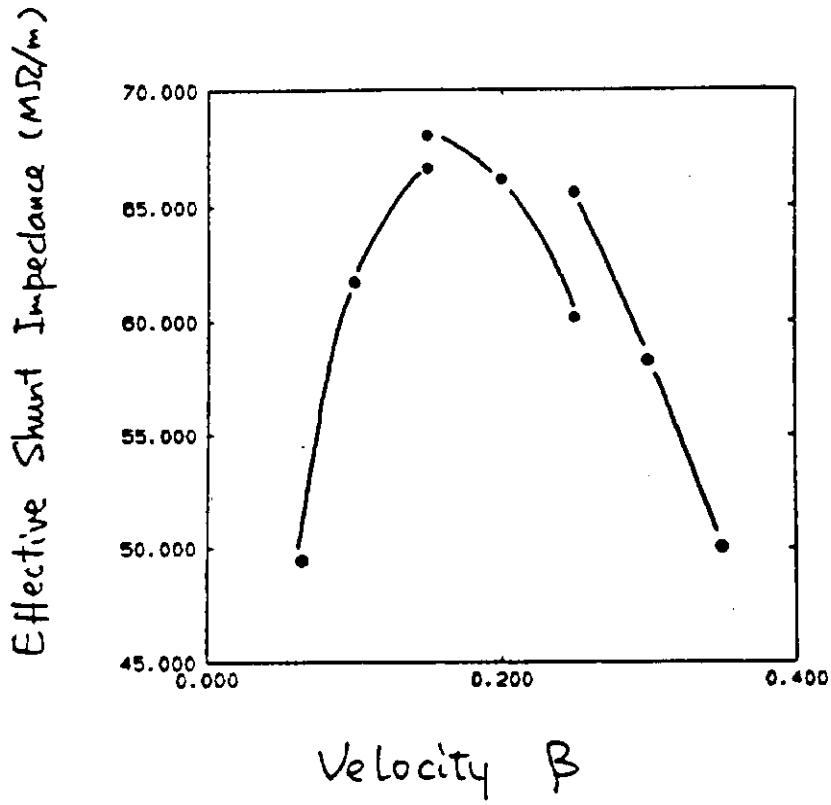
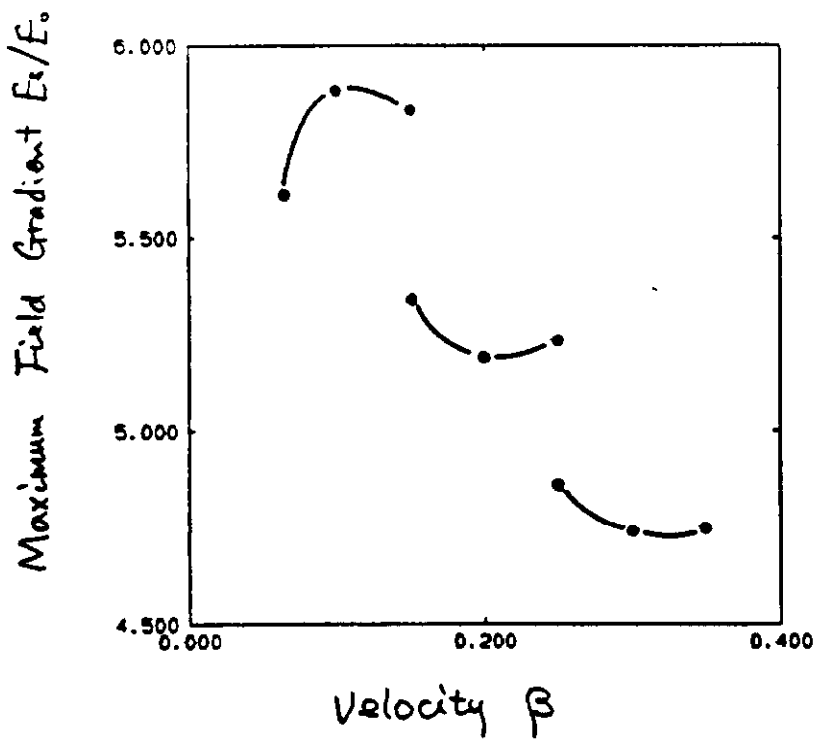


Fig. 17



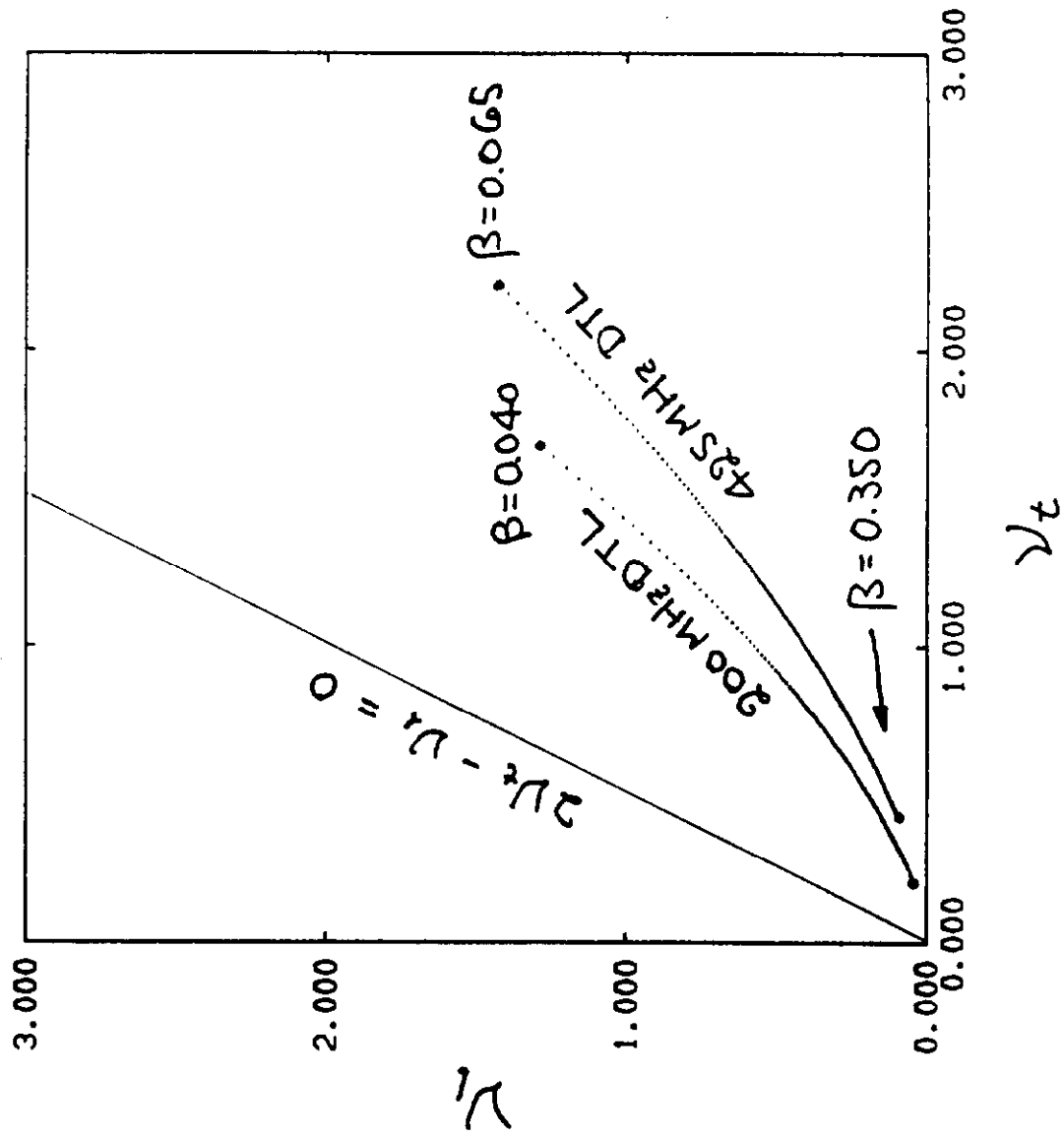


Fig. 18

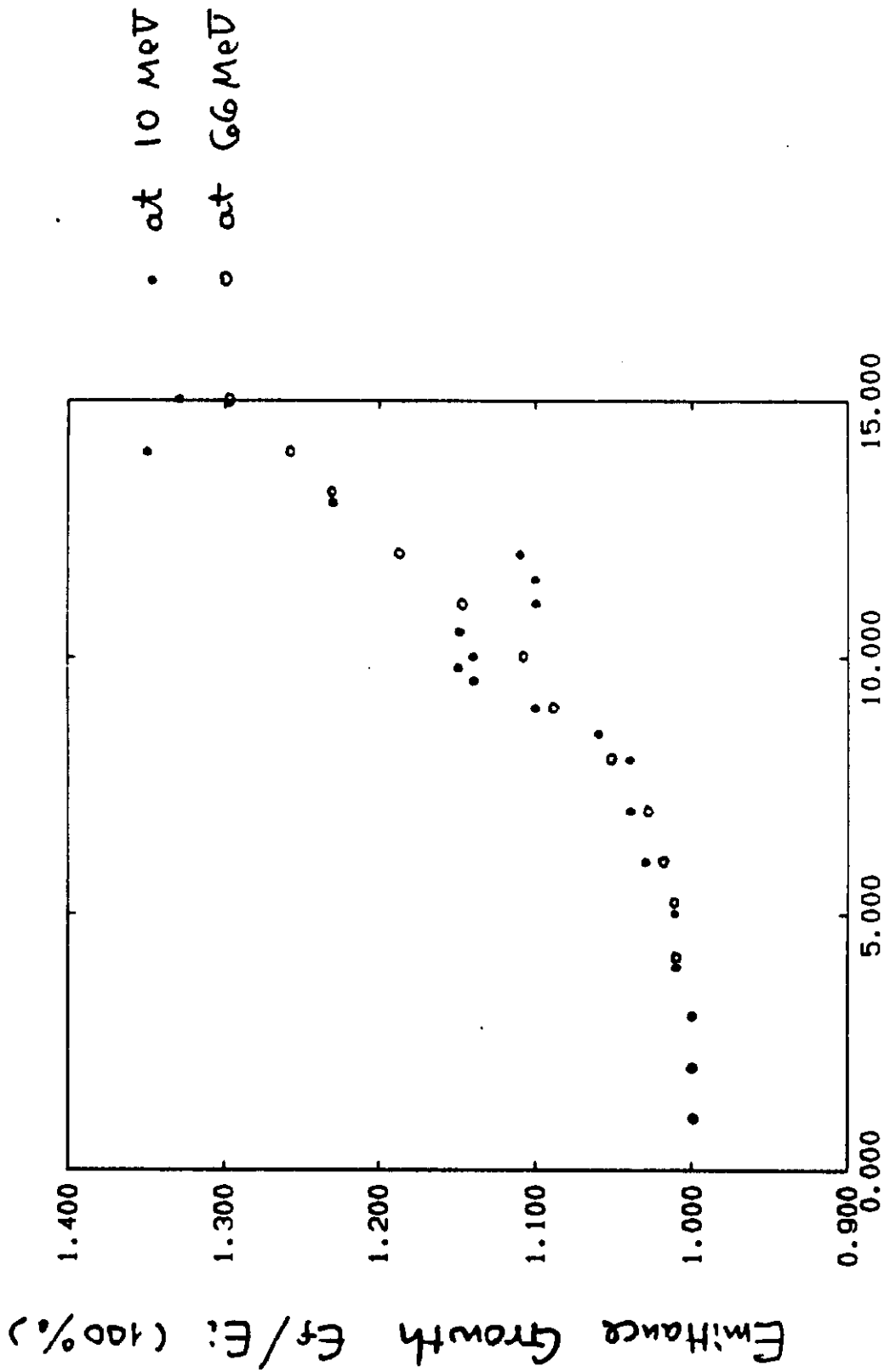


Fig. 19

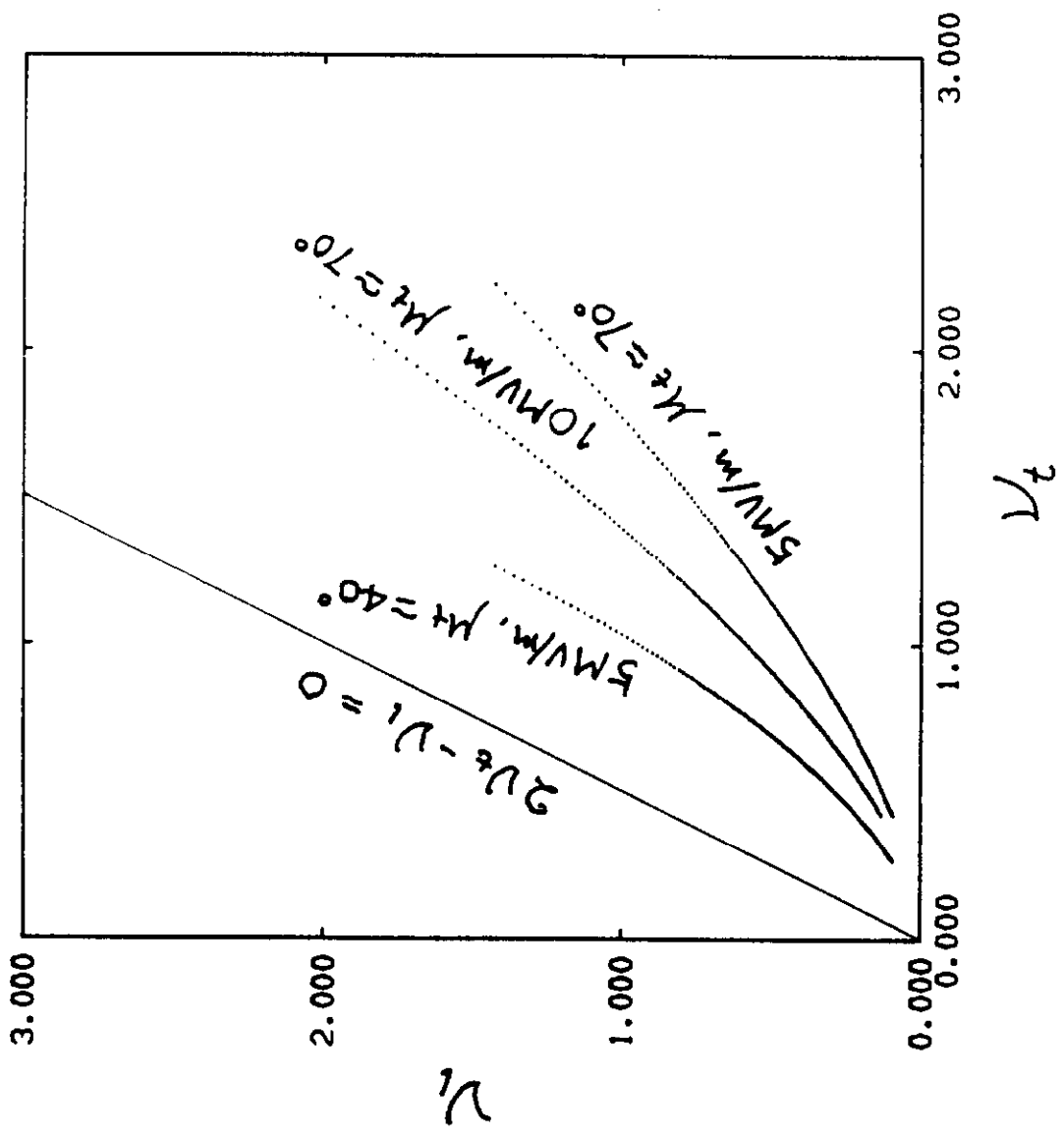
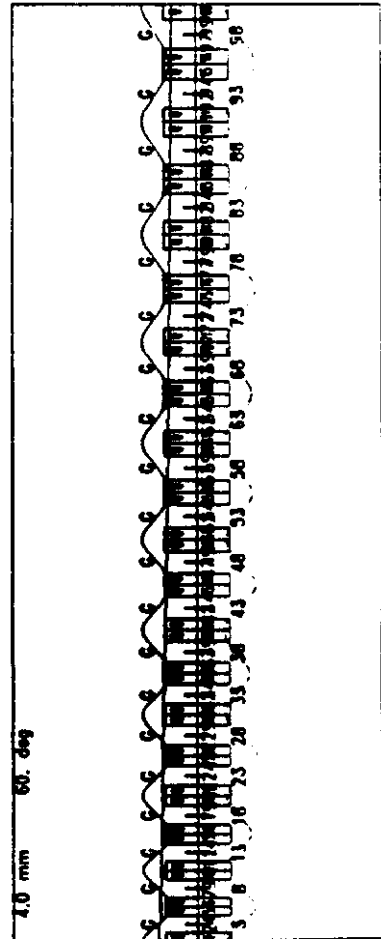
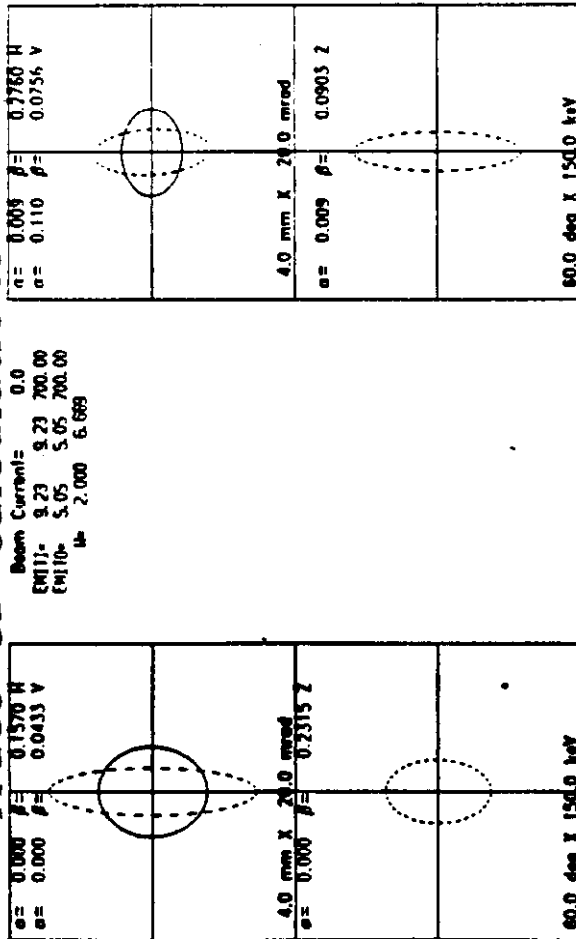


Fig. 20

Trace-3D Calculations

23-JUN-86 19:09:07



Trace-3D Calculations

23-JUN-86 19:12:00

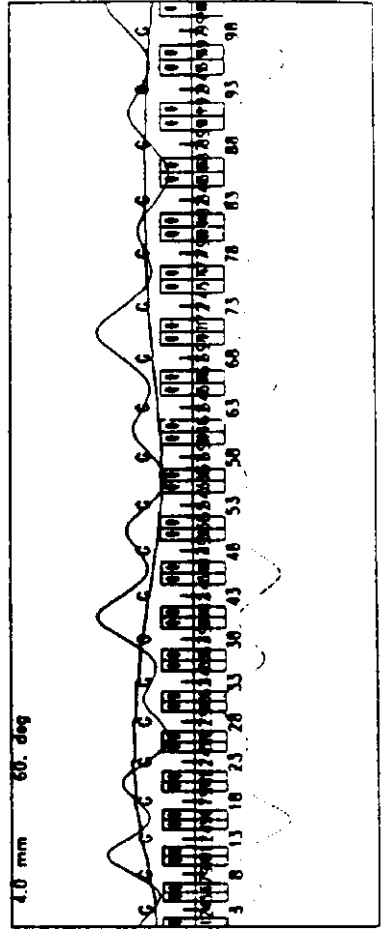
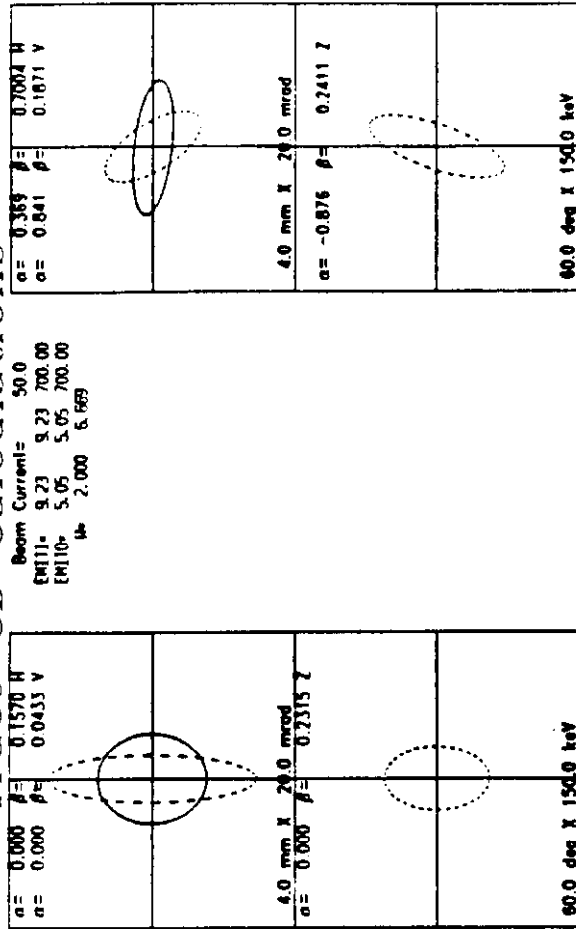


Fig. 21

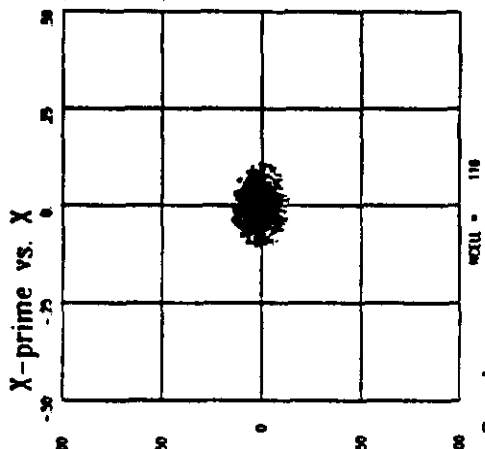
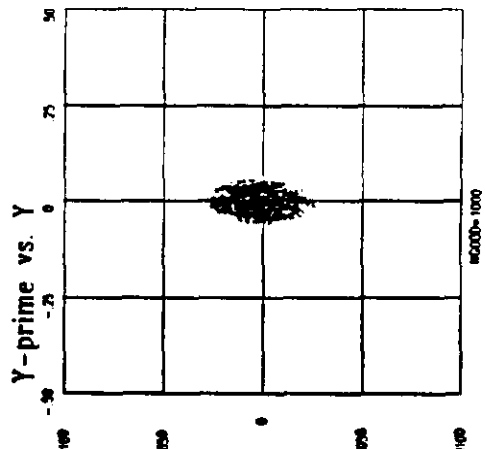
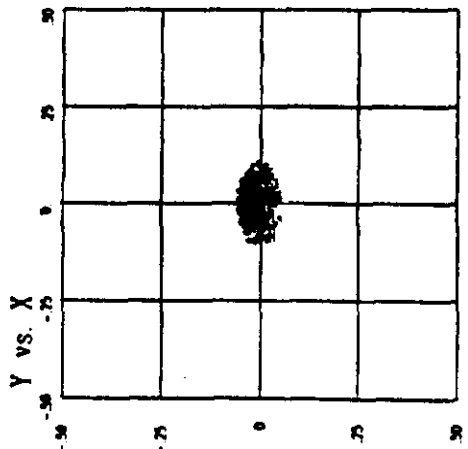
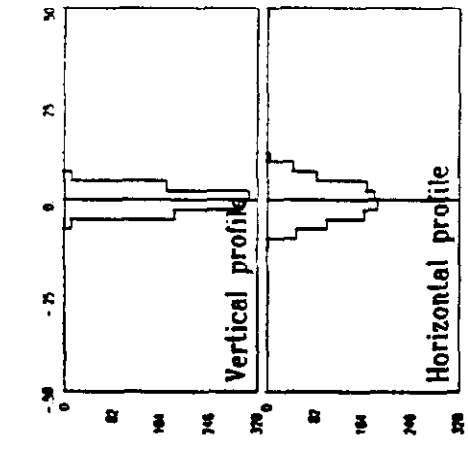
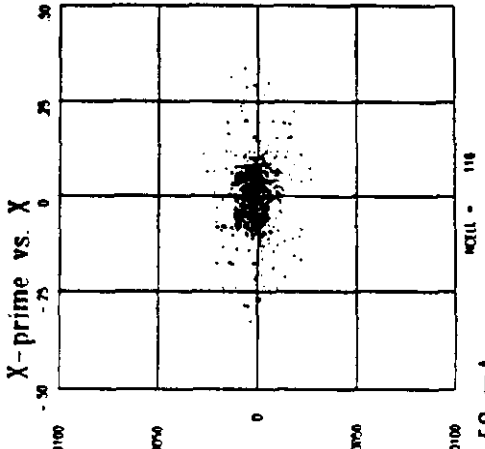
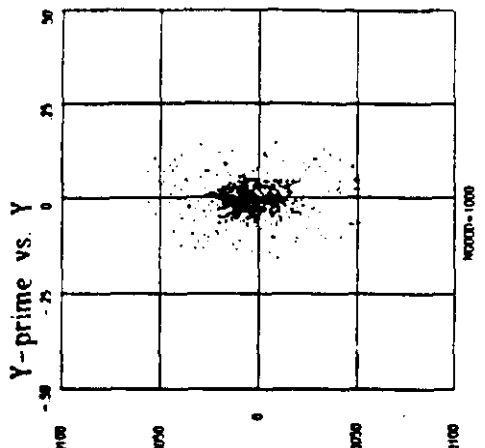
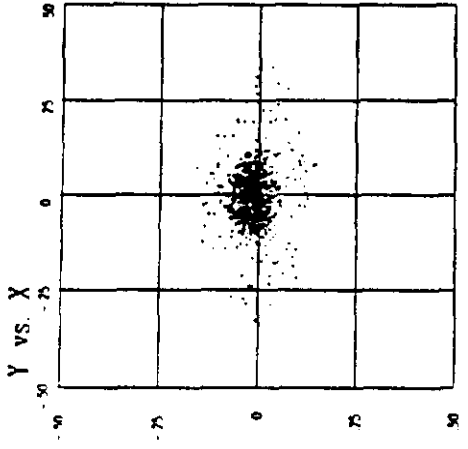
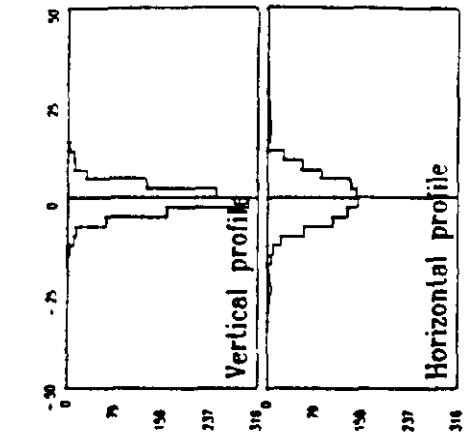


Fig. 22

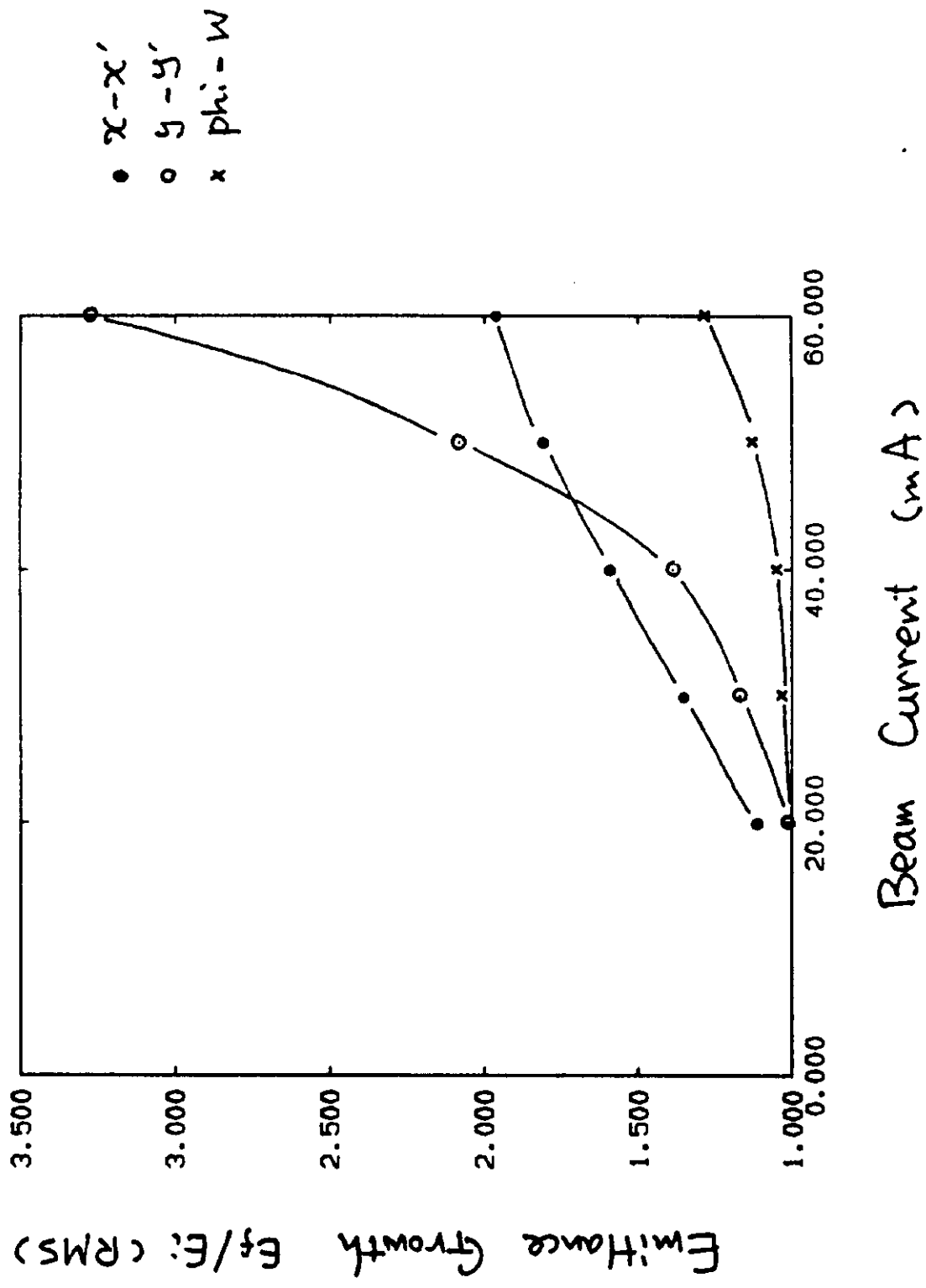
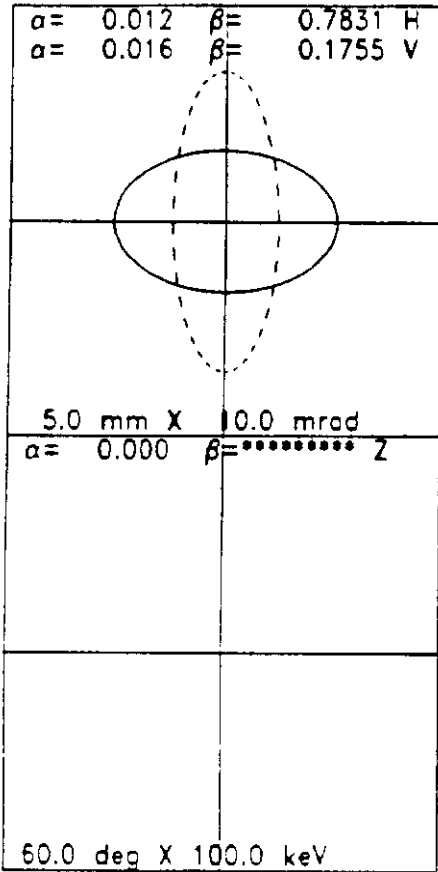
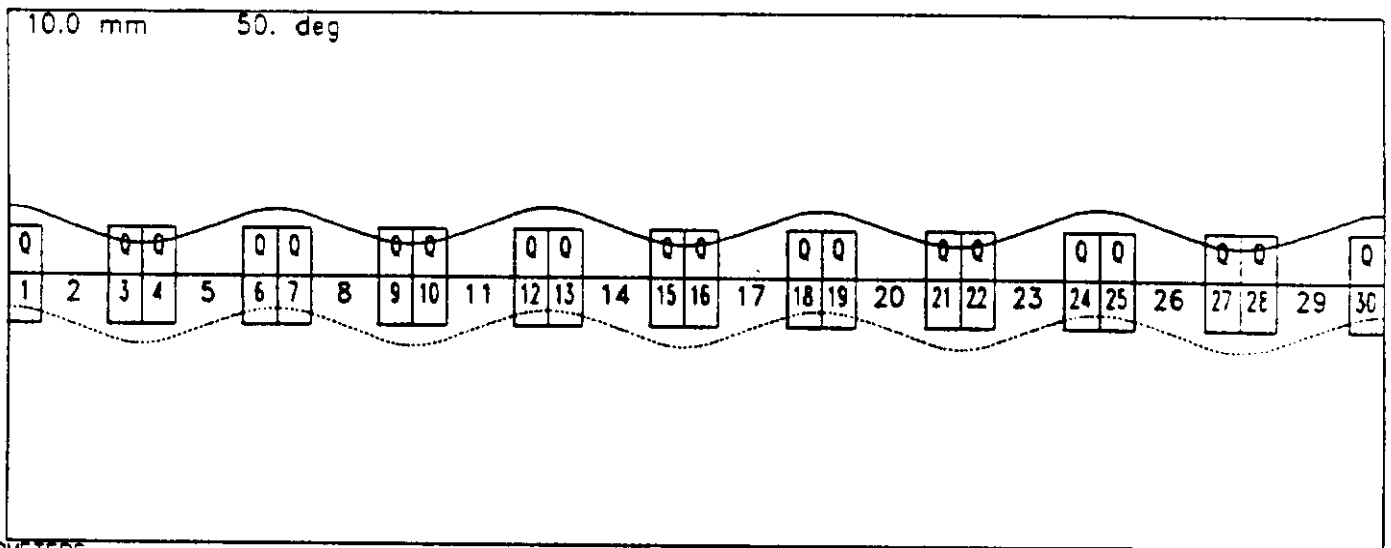
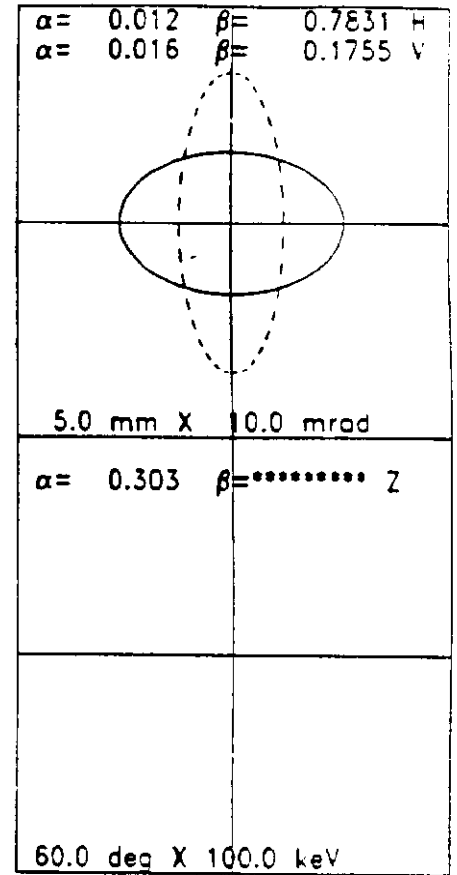


Fig. 23

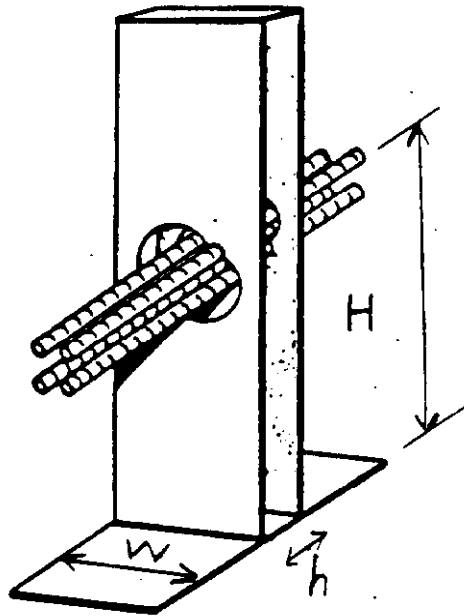


Beam Current= 50.0
 EMIT1= 8.57 8.57 900.00
 EMIT0= 8.57 8.57 900.00
 W= 2.300 2.300



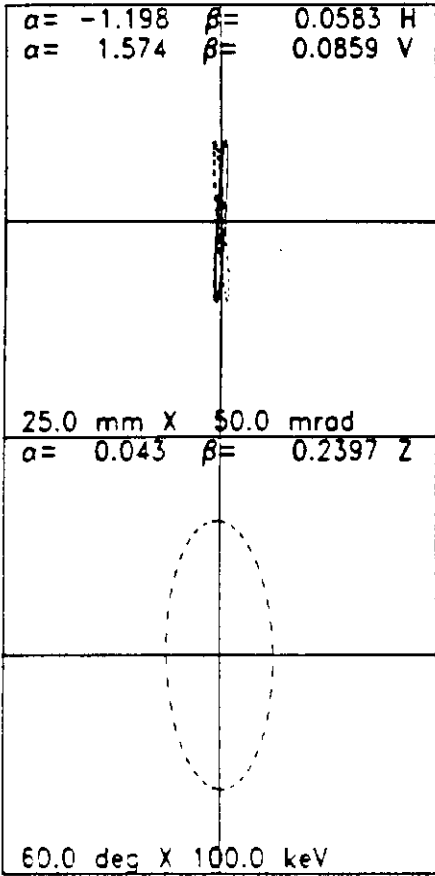
...TWISS PARAMETERS...

Fig. 24



Schematic of the twin-inductor 4-rod RFQ basic module developed at CRNL.

Fig. 25



Beam Current= 0.0
 EMITI= 8.57 8.57 900.00
 EMITO= 8.57 8.57 900.00
 W= 2.300 2.300

Phi= 148.6 deg, W= 2.300 MeV
 DP= 15.2 deg, DW= 59.695 keV
 DZ= 2.08 mm
 DP/P= 12.99 mrad
 EMITZ= 26.83 pi mm-mrad

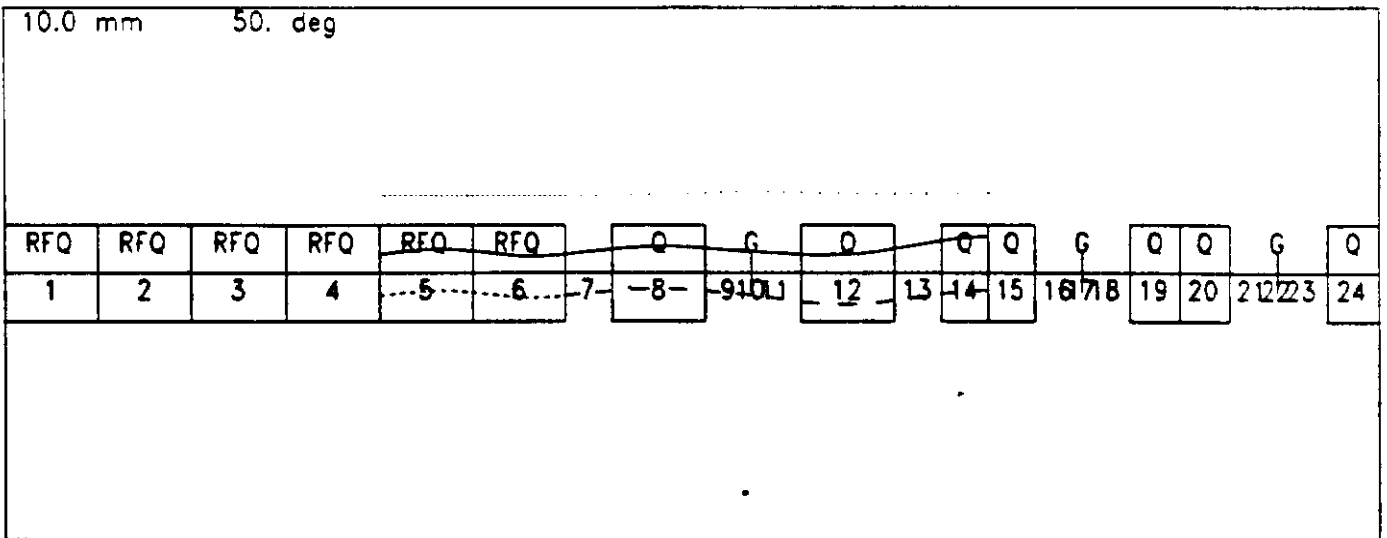
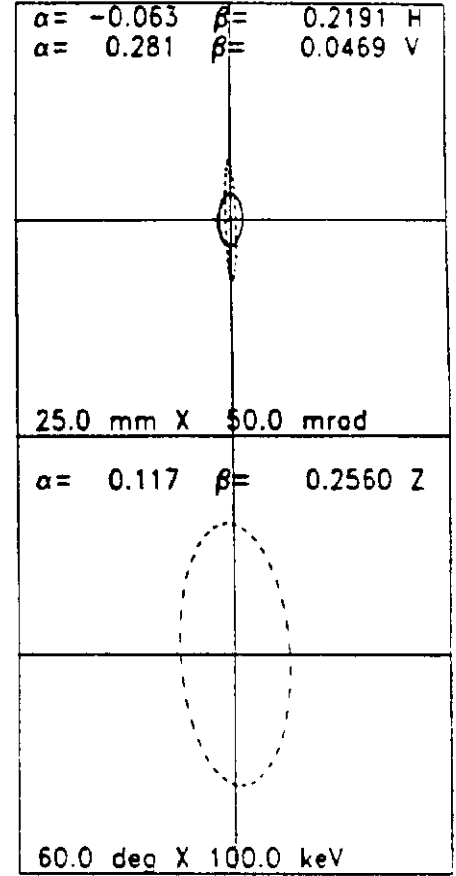


Fig. 26

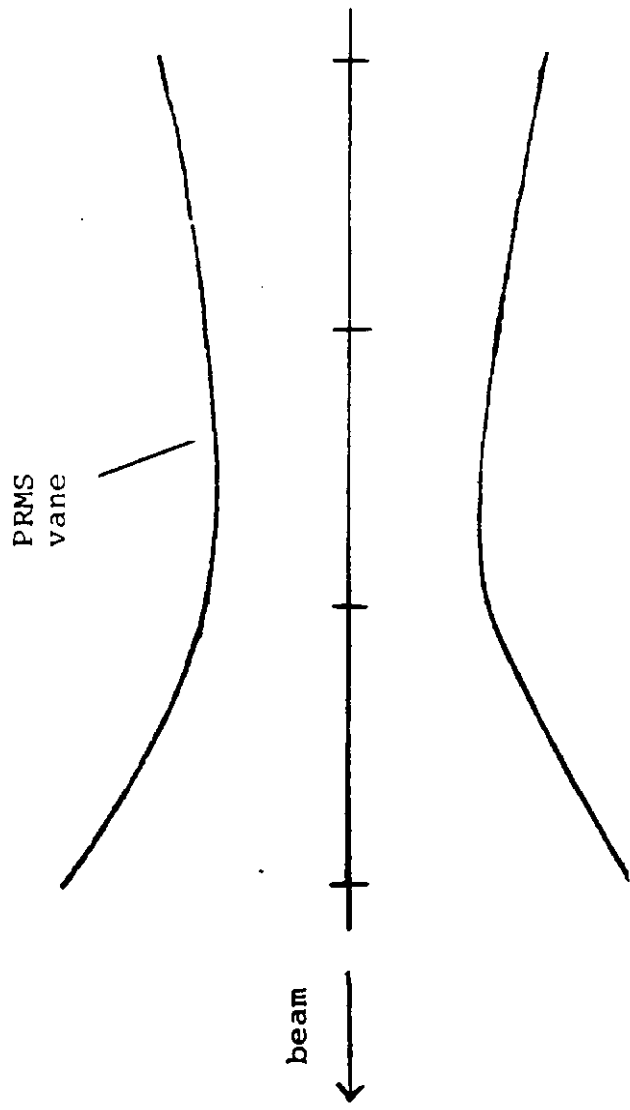
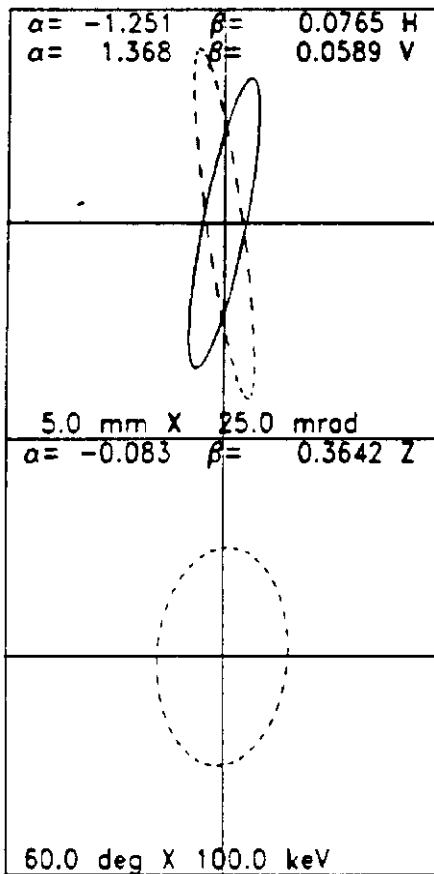


Fig. 27



Beam Current= 50.0
 EMIT1= 8.57 8.57 900.00
 EMIT0= 8.57 8.57 900.00
 W= 2.300 2.300
 Phi= 146.4 deg, W= 2.300 MeV
 DP= 29.2 deg, DW= 69.796 keV
 DZ= 4.00 mm
 DP/P= 15.19 mrad
 EMITZ= 26.83 pi mm-mrad

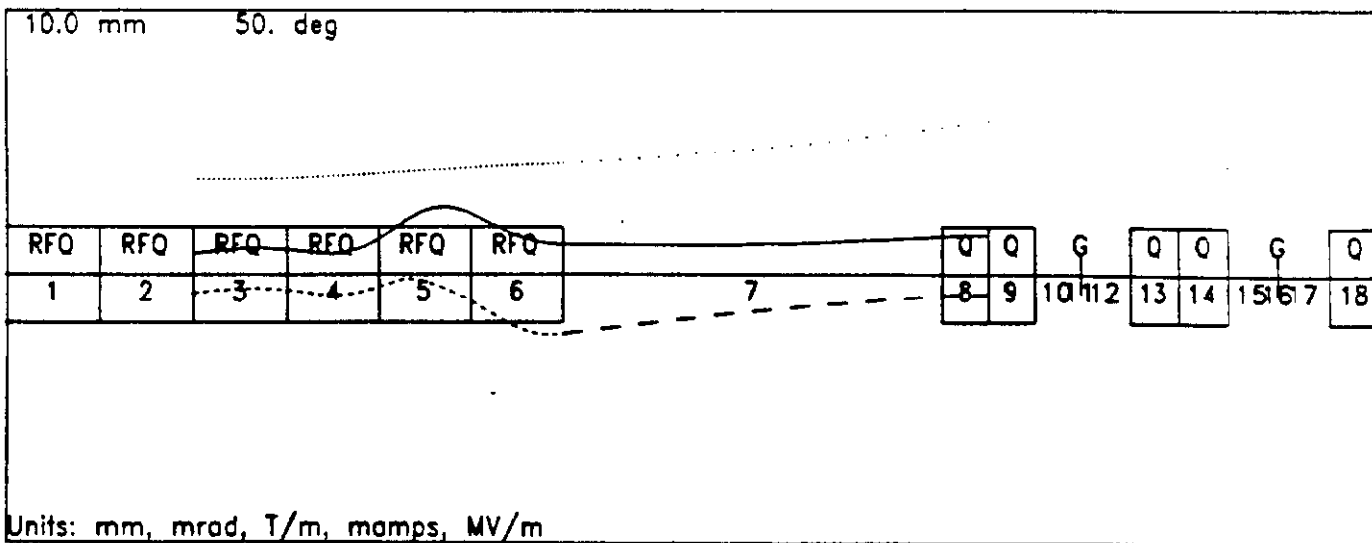
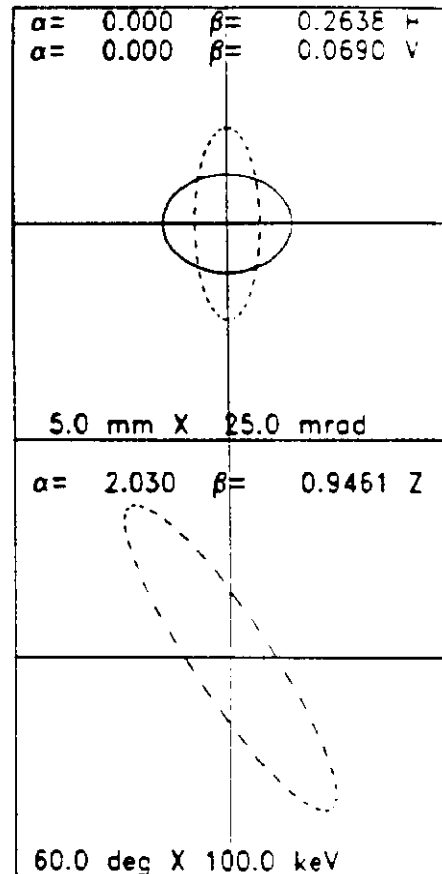


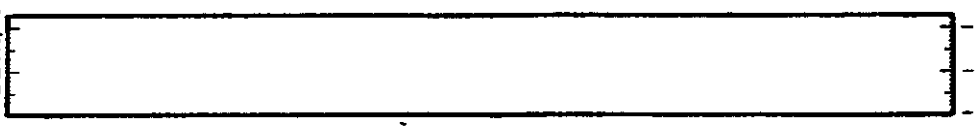
Fig. 28

66MEV DTL FOR MEDICAL USE 0.065; Resonant frequency= 425.415



Fig. 30

SUPERFISH DTL TEST PROBLEM BETA; Resonant frequency= 0.000



pill box

2/cm

8.29 cm

Fig. 29

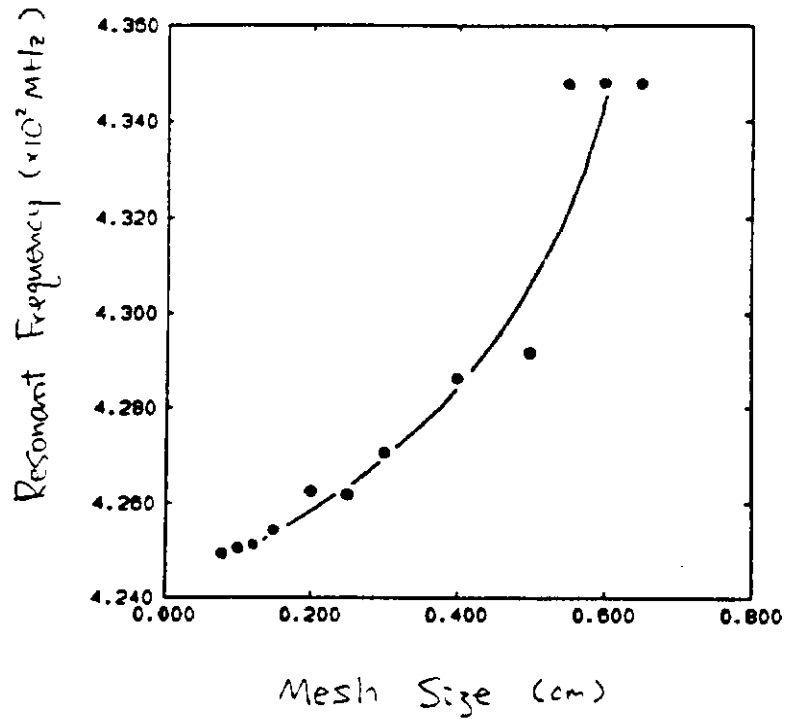


Fig. 31

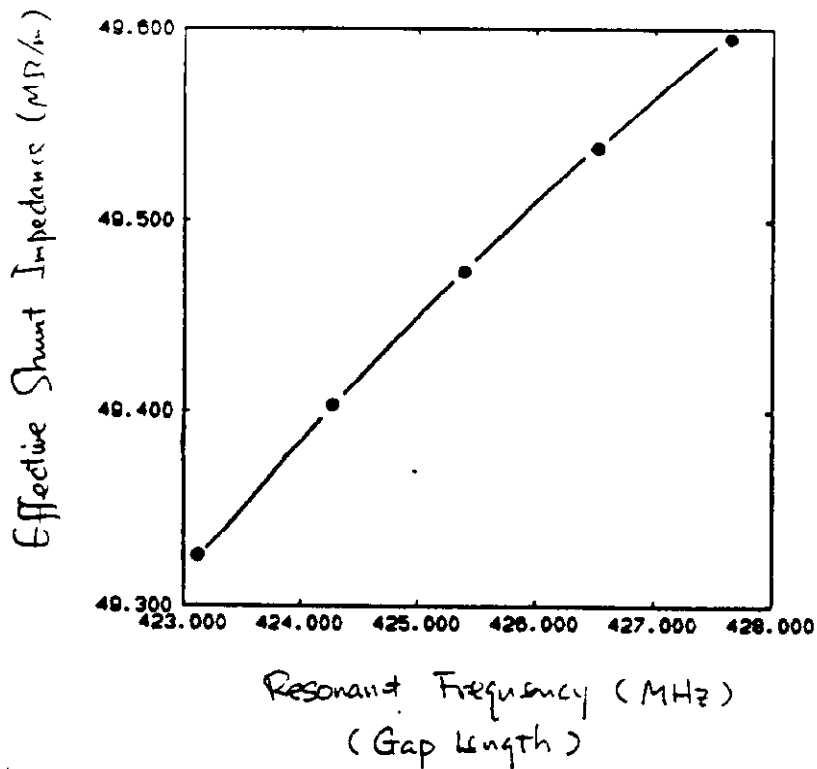
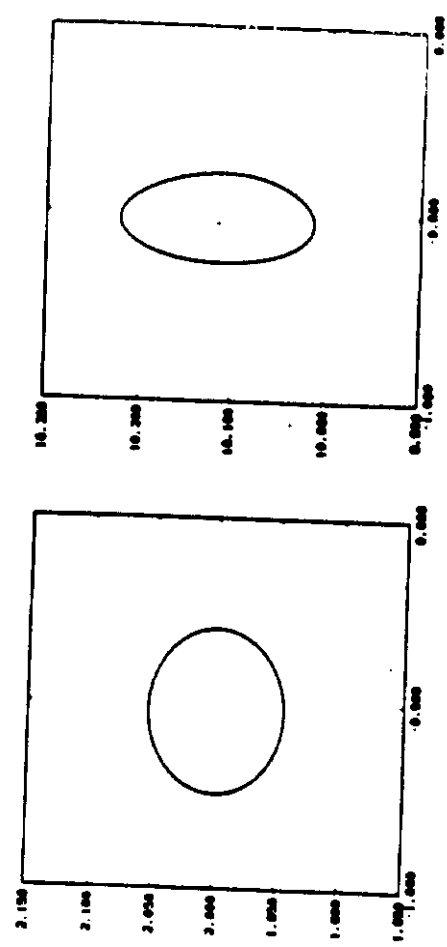
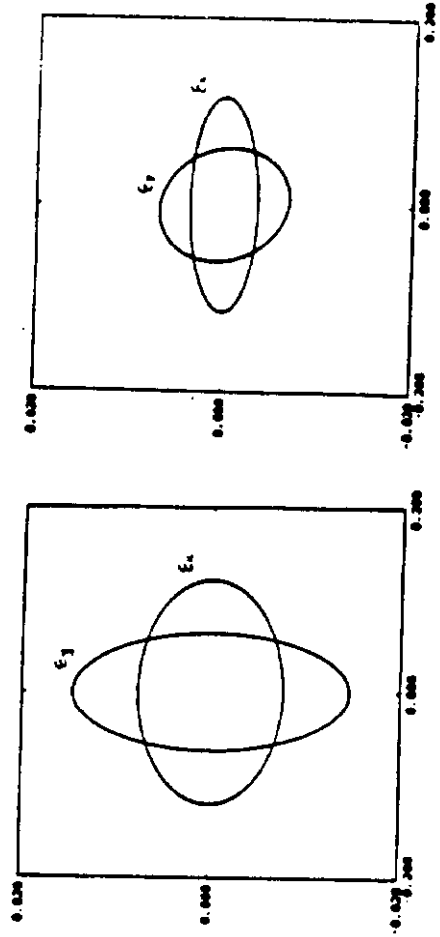


Fig. 32

2.0 MeV

10.1 MeV



output
 $E_{x,y} = 0.060 \pi \text{ cm} \cdot \text{mrad}$
 (hor.)
 $\alpha_x = -0.011$
 $\beta_x = 33.10 \text{ cm}$
 $\alpha_y = 0.125$
 $\beta_y = 8.78 \text{ cm}$

(TRACE)
 (0.06)
 (0.010)
 (33.47)
 (0.134)
 (8.76)

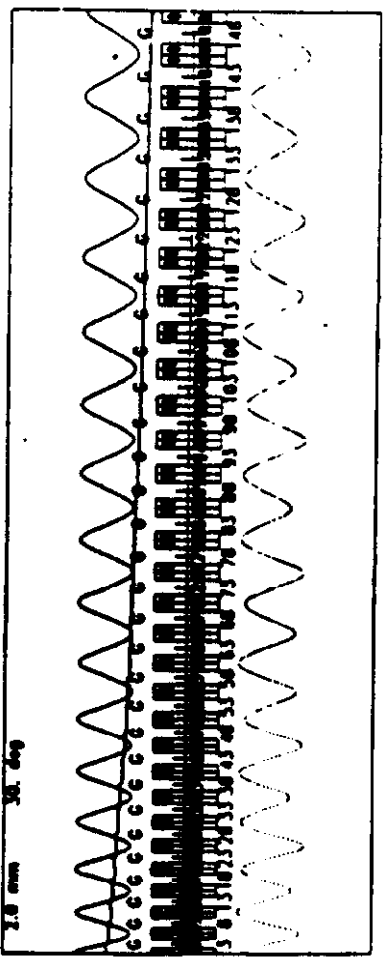
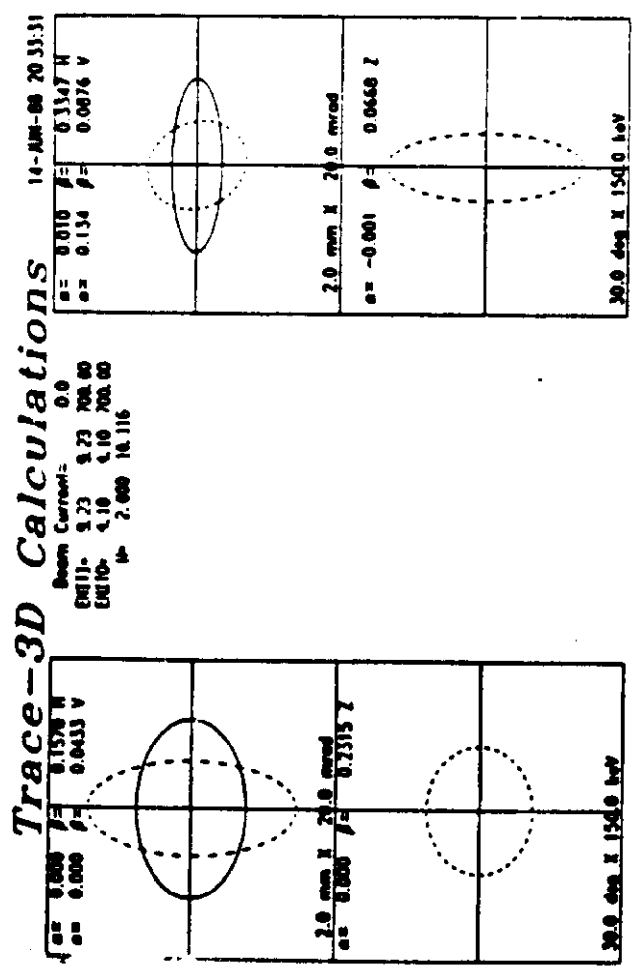


Fig. 33